Palaeogeography, Palaeoclimatology, Palaeoecology 540 (2020) 109526

Contents lists available at ScienceDirect

Palaeogeography, Palaeoclimatology, Palaeoecology

journal homepage: www.elsevier.com/locate/palaeo

High-resolution records of growth temperature and life history of two *Nacella* limpet species, Tierra del Fuego, Argentina

Adam Nicastro[a], Donna Surge[a,*], Ivan Briz i Godino[b,d,f], Myrian Álvarez[b], Bernd R. Schöne[c], Maria Bas[b,e]

[a] Department of Geological Sciences, University of North Carolina at Chapel Hill, Chapel Hill, NC, USA
[b] CONICET- Centro Austral de Investigaciones Científicas, Ushuaia, Argentina
[c] Institute of Geosciences, Johannes Gutenberg-Universität Mainz, Mainz, Germany
[d] Department of Archaeology, University of York, York, UK
[e] Department of Evolutionary Biology, Ecology and Environmental Science, Biodiversity Research Institute (IRBio), University of Barcelona, Barcelona, Spain
[f] DRCLAS at Harvard University, Cambridge, MA, USA

ARTICLE INFO

Keywords:
Sclerochronology
Oxygen and stable carbon isotopes
Temperature proxy
South America
Climate

ABSTRACT

Stable isotope ratios in patelloid limpets of the genus *Patella* have been established as proxies for coastal environmental change at sub-monthly resolution along the eastern North Atlantic and Mediterranean Sea. *Nacella deaurata* (Gmelin 1791) and *N. magellanica* (Gmelin 1791) are common intertidal species of patelloid limpets inhabiting the coast of Tierra del Fuego, Argentina/Chile and are commonly found in Holocene archaeological deposits. Here, we examine oxygen and carbon isotope ratios ($\delta^{18}O_{shell}$ and $\delta^{13}C_{shell}$, respectively) of modern specimens of *N. deaurata* and *N. magellanica* to test the hypotheses that: 1) they form their shells in isotopic equilibrium with ambient water; and 2) prominent growth lines form annually. Based on growth margin analysis of $\delta^{18}O_{shell}$ values, we identified a positive offset of 1.3 ± 0.4‰ (*N. deaurata*) and 1.3 ± 0.3‰ (*N. magellanica*) from expected equilibrium, similar to other patelloid limpets. Because the offset is relatively consistent between observed and expected values, it can be taken into account to reliably reconstruct growth temperature. Seawater temperature estimated from oxygen isotope time series data falls within the observed range. Thus, *N. deaurata* and *N. magellenica* shells serve as reliable proxy archives of seasonal variation in coastal seawater temperature. Time series of $\delta^{13}C_{shell}$ values do not vary seasonally in all shells; hence, the influence on its variation requires further study. The timing of prominent growth lines contextualized by the $\delta^{18}O_{shell}$ time series form twice a year and therefore cannot be used to estimate lifespan. Future isotopic analysis of archaeological *Nacella* shells can potentially provide much needed information about Holocene climate change at sub-monthly resolution from high-latitude South American locations, and contribute to our understanding of human behavior and human-climate interactions.

1. Introduction

Marine proxy archives are the foundation for extrapolating changes in oceanographic conditions beyond the bounds of the instrumental record. Currently, records of paleoclimate in the Southern Ocean are relatively scarce when compared to records of paleoclimate from other ocean basins. Many of the limited paleoclimate proxy records in the Southern Ocean are derived from ice, marine, or lake sediment cores (Borromei and Quattrocchio, 2001; Borromei et al., 2010; Mauquoy et al., 2004; Candel et al., 2009; Ponce et al., 2017). These records, while temporally extensive, focus on centennial to millennial time scales. Few of these proxy records capture changes to coastal environments, which are particularly sensitive to changing climate conditions. Even fewer paleoclimate data exist at decadal, annual, and seasonal time scales along coastlines in the Southern Ocean. Hence, a proxy record that can be resolved to sub-monthly resolution is necessary to understand seasonal variability in coastal environments from high southerly latitudes.

Stable isotopes in mollusc shells have been used to reconstruct paleoclimate records to sub-monthly resolution. Most molluscs form their shells in isotopic equilibrium with ambient water (Epstein et al., 1951, 1953; Craig, 1957; Grossman and Ku, 1986), but this is not always the

* Corresponding author at: University of North Carolina at Chapel Hill, Department of Geological Sciences, 104 South Road, CB #3315, Chapel Hill, NC 27559-3315, USA.
E-mail address: donna64@unc.edu (D. Surge).

https://doi.org/10.1016/j.palaeo.2019.109526
Received 9 August 2019; Received in revised form 6 December 2019; Accepted 9 December 2019
Available online 13 December 2019
0031-0182/

case. Previous studies have shown that limpet species from the genus, *Patella*, form their shells in isotopic disequilibrium with ambient water (e.g. Shackleton, 1973; Cohen and Tyson, 1995; Fenger et al., 2007; Ferguson et al., 2011; Surge et al., 2013; Parker et al., 2017; Prendergast and Schöne, 2017). In these studies, seawater temperatures were reliably reconstructed after subtracting a consistent, positive offset in $\delta^{18}O_{shell}$ values relative to expected equilibrium values. Thus, if such offsets from expected equilibrium values are consistent in modern specimens, it can be accounted for to reliably reconstruct sea surface temperature (SST) in older (i.e., archaeological or fossil) specimens (Surge and Barrett, 2012; Wang et al., 2012).

Other studies examined stable isotope ratios in mollusc shells to understand life history and growth patterns (Jones, 1983; Jones et al., 1984, 1989; Jones and Quitmyer, 1996; Goodwin et al., 2001). In particular, studies of patelloid limpets have noted prominent growth lines that occur annually, possibly due to growth temperature stress in winter and/or summer, reproductive stress, or changes in food supply (Fenger et al., 2007; Surge et al., 2013; Ambrose Jr. et al., 2016). As such, prominent growth lines can help to contextualize the growth patterns and lifespans of a shelled animal, provided that the timing of prominent growth formation is understood.

Here, we interpret records of life history and seasonal variation in growth temperature preserved in modern specimens of two high-southerly latitude limpets, *Nacella deaurata* (Gmelin, 1791) and *N. magellanica* (Gmelin, 1791). Through the analysis of oxygen and stable carbon isotope ratios ($\delta^{18}O_{shell}$ and $\delta^{13}C_{shell}$, respectively), we test the hypotheses that: 1) these species form their shells in isotopic equilibrium with ambient water; 2) their shells record seasonal variation in SST; and 3) prominent growth lines in their shells form annually. Our results have implications for an important new and abundant resource for studying human behavior, past climate change, and ultimately human-climate interactions from high southerly latitudes in South America (Álvarez et al., 2018).

2. Materials and methods

2.1. Ecology of Nacella deaurata and N. magellanica

Nacella deaurata and *N. magellanica* are intertidal patelloid limpets that inhabit coastal areas of the Magellanic Province, which wraps around the southern tip of South America from Chiloé through Cape Horn, Atlantic Southern Patagonia Coast, Tierra del Fuego Archipelago, and the Malvinas/Falkland Islands (Spalding et al., 2007). The two species can be differentiated using several morphological features such as shell height, sculpture, and mantle tentacle pattern (Valdovinos and Ruth, 2005). *Nacella magellanica* shells are typically taller than *N. deaurata* shells, with a more rounded sculpture pattern at the shell margin (Fig. 1a). These two species live from 0 to 30 m depth (Valdovinos and Ruth, 2005). *Nacella deaurata* lives in the lower intertidal and sublittoral zones, while *N. magellanica* lives mostly in the high and middle intertidal zones. As a result, *N. magellanica* are exposed subaerially twice daily for 3–5 h, whereas *N. deaurata* are exposed once a day only during spring tides. Consequently, *N. magellanica* is subjected to more extreme temperatures ranging from 0 to 20 °C. In contrast, *N. deaurata* experiences temperatures between 4 and 11 °C (Morriconi and Calvo, 1993; Morriconi, 1999). Both species source their diets primarily from the middle and low intertidal zone, and feed when submerged. *Nacella deaurata* subsists primarily on macroalgae, whereas *N. magellanica* subsists primarily on invertebrates and microalgae (Rosenfeld et al., 2018). Both species typically have one major spawning event per year. Reproductive organs begin to mature as water temperature starts to rise, with a peak spawning event occurring in late spring (November/December) (Morriconi, 1999; Morriconi, 2005). Minor spawning events sometimes occur as water temperatures begin to rise in early spring (Morriconi, 2005).

2.2. Geographic and oceanographic settings

The Beagle Channel (54.8–55°S, 67.2–70°W) is a narrow waterway in the Tierra del Fuego Archipelago at the southern tip of South America. It extends approximately 240 km from the Argentinian province of Tierra del Fuego in the east to the western coast of the Chilean Province of Magallanes. This study is set in the eastern portion of the Beagle Channel, 64 km east of Ushuaia, Argentina (Fig. 2). This Argentinean portion of the Beagle Channel coast has a long tradition of archaeological, biological, and climatic research, offering rich sampling opportunities related to archaeological shell middens, peatlands, and marine sediments to develop paleoclimate studies (Orquera and Piana, 2009; Vila et al., 2007; Mauquoy et al., 2004; Borromei et al., 2010.) Gordillo et al. (2015) reports monthly mean SST values from Ushuaia Bay over a period of approximately 50 years ranging from approximately 4–9 °C (estimated from their Fig. 5; standard deviations not provided). Graniero et al. (2016) reports average salinity of 30.6 ± 0.8 psu (practical salinity units) at the study site, with little seasonal variation. Precipitation averages 570 mm per year, with more precipitation generally occurring in winter than in summer (Gordillo et al., 1992).

Waters of the Beagle Channel are influenced by the Antarctic Circumpolar Current (ACC), the strength of which is determined by the strength of the Southern Hemisphere Westerly Winds (SHWW). The primary cause of climate variation in the study area is the Southern Annular Mode (SAM; Limpasuvan and Hartmann, 1999), also known as the Antarctic Oscillation (AAO, Gong and Wang, 1999). The SAM index is defined as the difference in mean sea-level pressure (MSLP) between 40°S and 65°S latitude (Gong and Wang, 1999). During positive phases of SAM, MSLP is higher at mid latitudes than at high latitudes, causing the SHWW to contract toward Antarctica. During negative phases of SAM, MSLP is higher at high latitudes than at mid latitudes, causing the SHWW to expand toward the southern edges of South America, Africa, and Australia. In southern South America, positive phases of SAM are associated with warmer, drier conditions, while negative phases coincide with colder and wetter conditions (Thompson and Solomon, 2002; Sen Gupta and England, 2006; Gillett et al., 2006; Dätwyler et al., 2018). SAM oscillates between positive and negative phases over periods between several months to approximately five years (Marshall, 2003). SAM oscillation since 1980 is shown in Fig. 3, with shell collection years identified by open symbols.

The study area contains a long history of human habitation recorded in archaeological shell middens, of which *N. deaurata* and *N. magellanica* are major constituents (Colonese et al., 2012; Zurro et al., 2017). Archaeological shells within middens provide not only evidence of human harvesting patterns, but also archives of paleoenvironmental change. Middens in the area date from 6500 BP to the 20th century (Estevez et al., 2001; Orquera et al., 2011). Therefore, archaeological shells in local middens potentially provide a rich archive of Late Holocene climate variability in southern South America, as well as providing information on the preferred season of harvest of fish and shellfish of past societies.

2.3. Shell collection and water measurements

Live specimens of *N. deaurata* and *N. magellanica* and water samples were collected monthly from the Lanashuaia location, in the Beagle Channel, Tierra del Fuego, Argentina (54°52′50.07″ S, 67°16′25.27″ W) from October 2015 to October 2016. The study site was inaccessible due to snow in August 2016; thus, no shells or water were collected that month. Shells were collected from Bahía Cambaceres Exterior (Outer Cambaceres Bay), the seaward side of a narrow isthmus separating this Bay from Bahía Cambaceres Interior (Inner Cambaceres Bay). Between 7 and 10 live individuals of each species were collected at each sampling date. Shells were selected based on size (total height from margin to apex, and length from anterior to posterior), as well as shell

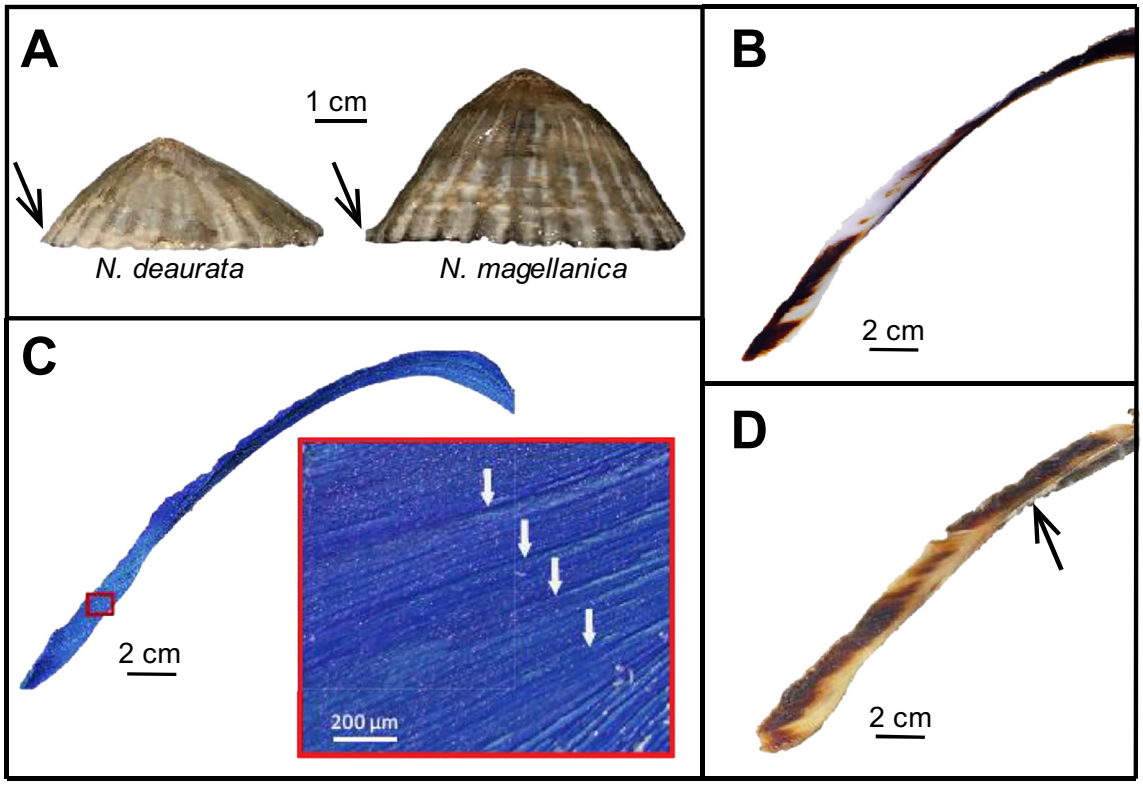

Fig. 1. A) Photographs of *Nacella deaurata* and *N. magellanica*. Note differences in height and sculpture between the two species. Black arrows indicate the anterior growth margin, where monthly-collected shells were sub-sampled. B) Image of polished cross-section of *N. magellanica* posterior growth axis showing natural pigmentation. C) Image of cross-sectioned *N. deaurata* shell treated with Mutvei's solution. The inset is an enlarged portion of the image to the left. White arrows in the inset indicate bundles of 10–14 micro-growth lines. *Nacella magellanica* shows the same packaging of micro-growth increments. D) Representative image of cross-sectioned *N. deaurata* shell treated with Feigl's solution. The black arrow indicates the aragonitic portion of the shell stained by Feigl's solution. This procedure identified a similar location of the aragonitic layer in *N. magellanica*.

thickness. Shells with chipped or cracked margins were avoided. Limpets were pried from the rocks in the intertidal zone at low tide, and care was taken to not damage the growing edge. The specimens were transported to the laboratories at Centro Austral de Investigaciones Científicas (CADIC-CONICET), Ushuaia, Argentina. Live specimens were stored in a refrigerator at 3–4 °C for no more than a day before the animal was removed from the shell. Viscera were removed after immersion in hot water for 20 to 30 s. Water used to remove the animal from the shell was never hot enough to boil the animal or its shell.

Temperature and salinity of local water was measured at each of the collection dates using a multi-parameter water quality monitor (Hannah Instruments 9828) with a precision of ± 0.15 °C and ± 0.01 psu, respectively. Water for oxygen isotope analysis measurements was collected in 30 ml glass vials and filled to the top to avoid any headspace. Isotopic analytical methods of water samples are described below in Section 2.5.

2.4. Analysis of shell microstructure and mineralogy

Shell growth lines, microstructure, and mineralogy were examined using acetate peels, Mutvei's solution, and reflected-light microscopy. Shells were sectioned from anterior to posterior along the axis of maximum growth using a Buehler IsoMet low-speed saw and mounted onto glass slides using Gorilla Glue clear epoxy. Cross-sectioned shells were ground to a flat surface using a 600 grit silicon carbide grinding paper (BuehlerMet II). Samples were then polished using a 6 µm diamond suspension grit followed by a 1 µm diamond suspension grit (Buehler). Digital images of the sectioned shells were captured using an Olympus DP71 Camera mounted to an Olympus SZX7 microscope, and Olympus StreamEssentials software for Windows v2.2 (Fig. 1B). Image resolution was 4080 × 3072 pixels. Acetate peels of the sectioned shells were prepared following the methods described in Carter and Ambrose (1989) to identify growth lines and assess microstructure type.

Shells were treated with Mutvei's solution to enhance the visibility of prominent growth features. Mutvei's solution was prepared according to the methods described by Schöne et al. (2005a). Shell sections were cleaned ultrasonically in deionized water, rinsed in ethanol, and allowed to air dry. Samples were immersed in the Mutvei's solution which was kept at a temperature between 37 and 40 °C under constant stirring for about 1 h. The shell sections were then removed from the solution, rinsed with deionized water, and allowed to air dry. Shells treated with Mutvei's solution were viewed and photographed using the same methods described above (Fig. 1C).

Feigl's solution was applied to shells that had not been treated with Mutvei's solution to differentiate calcite from aragonite within the shell (Fig. 1B). Feigl's solution was prepared according to methods outlined in Feigl (1958). The solution differentiates calcite from aragonite due to the different solubilities of the two minerals. Silver and manganese ions in Feigl's solution react with $OH\cdot^{-}$ ions produced from the dissolution of $CaCO_3$ in water. This process causes the shell material to change from its original color to a shiny black or silver (Fig. 1D). Aragonitic parts of the shell are more soluble and, therefore, change color more quickly than calcitic layers when treated with Feigl's solution. Polished shell sections were immersed in Feigl's solution for 1–2 h and periodically inspected until changes in shell color were visible.

2.4.1. Sampling along shell growth margin

Three shells from each collection date were selected for sampling along the growing edge for a total of 33 shells. Shells were selected based on shell thickness and preservation of the shell margin.

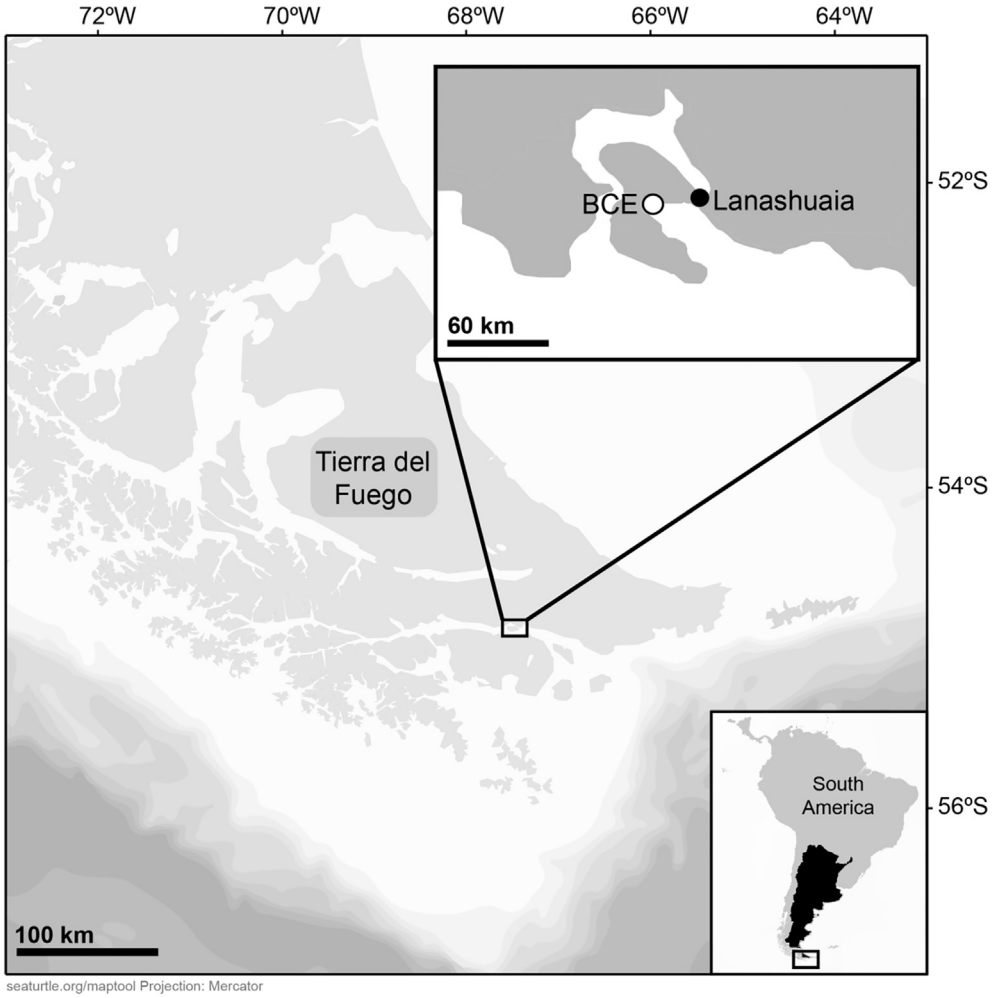

Fig. 2. Map of study area in the Beagle Channel, Tierra del Fuego, Argentina. The open circle indicates the shell collection site, Bahía Cambaceres Exterior (BCE). The filled circle identifies location of Lanashuaia where water samples were collected. The box shows the location of the study area relative to the country of Argentina (black shaded area in the lower-right inset map) and the continent of South America.

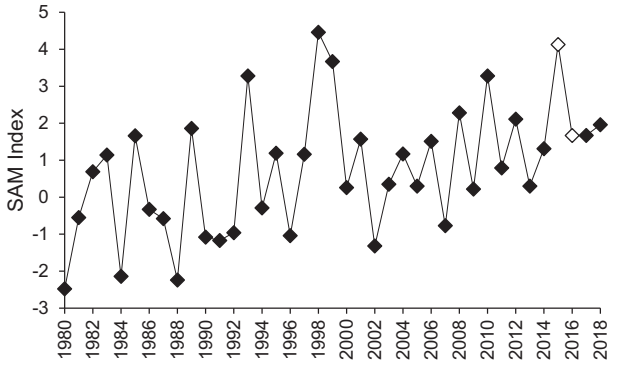

Fig. 3. Oscillation in SAM from 1980 to 2018. Each data point represents the annual average Southern Annular Mode (SAM) index for that year. The open symbols indicate the SAM index corresponding to the years during which shell specimens were collected. Data are provided by the British Antarctic Survey (https://legacy.bas.ac.uk/met/gjma/sam.html).

Specimens showing fragmentation, alteration, or fractures along the anterior growing edge were not selected. Approximately 100 μg of powdered carbonate material was milled from the anterior growth margin (Fig. 1A) of each selected shell using a hand-held Volvere VMAX Dental Drill with a fine-point breaking-contact drill bit (Brasseler Diamond, catalog number: 8859). The milled powder was sent to the University of Arizona's Environmental Isotope Laboratory for stable isotopic analyses. The isotopic analytical methods are described below in Section 2.5.

2.4.2. Serial sampling along maximum axis of growth

Six shells (three *N. deaurata* and three *N. magellanica*) from the last shell collection date (October 1, 2016) were chosen for serially sampling along the posterior half of the maximum axis of growth to produce a sub-monthly isotopic time series. Shells were selected based on visibility of prominent growth lines and shell thickness. Shells were sectioned from anterior to posterior along the axis of maximum growth and prepared following the methods described above. Shell cross-sections were microsampled at 150 to 200 μm intervals from the posterior growth margin toward the apex (9 to 10 cm) using a Merchantek Micromill with a scribe-point drill bit (Brasseler Carbide, catalog number: H1621). Powdered shell material from two shells (specimens ND-1016-4 and NM-1016-3) were sent to the Institute of Geosciences at the University of Mainz for stable isotopic analysis. The remaining four shells (ND-1016-1, ND-1016-3, NM-1016-1, NM-1016-5) were sent to the University of Arizona's Environmental Isotope Laboratory for stable isotopic analyses. The isotopic analytical methods are described below in the next section. Note that specimen identification numbers reflect species (ND = *N. deaurata*, NM = *N. magellanica*), collection month and year (1016 = October 2016), and individual out of the 5 specimens collected that month.

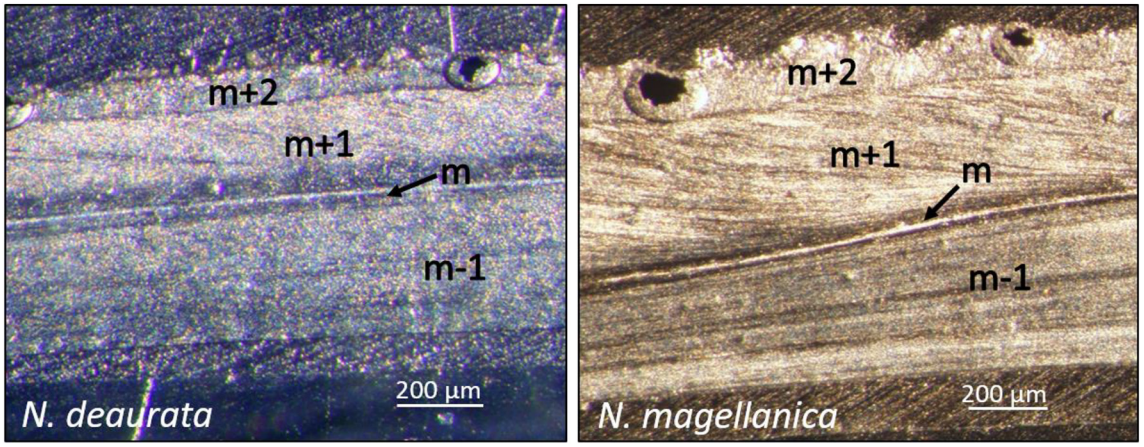

Fig. 4. Images of acetate peels of *Nacella deaurata* (left) and *N. magellanica* (right). The myostracum is denoted by the letter "m" and an arrow. Layers above and below are denoted by m + 1, m + 2, and m-1, depending on their dorsal or ventral position relative to the myostracum following MacClintock (1967).

2.5. Geochemical analyses

Water $\delta^{18}O$ values were measured at the Environmental Isotope Laboratory, University of Arizona on a dual inlet mass spectrometer (Finnigan Delta-S). Samples were equilibrated with CO_2 gas at approximately 15 °C in an automated CO_2-H_2O equilibration device coupled to the mass spectrometer. Standardization is based on internal standards referenced to Vienna Standard Mean Ocean Water 2 (VSMOW2, $\delta^{18}O$ = 0.00‰) and Standard Light Antarctic Precipitation 2 (SLAP2, $\delta^{18}O$ = −55.50‰). Precision is better than 0.08‰ (1σ).

Powdered shell material sent to the University of Arizona's Environmental Isotope Laboratory was measured using an automated carbonate preparation device (KIEL-III) coupled to an isotope ratio mass spectrometer (Finnigan MAT 252). Powdered samples were reacted with dehydrated phosphoric acid under vacuum at 70 °C. The isotope ratio measurement is calibrated based on repeated measurements of NBS-19, NBS-18, and CAR-1, an in-house carbonate standard. The following isotope ratios are assigned to these standards ($\delta^{18}O$ followed by $\delta^{13}C$): NBS-19, −2.20‰, +1.95‰; NBS-18, −23.20‰, −5.01‰; CAR-1, −1.41‰, +2.03‰. Analytical precision is ± 0.10‰ for $\delta^{18}O$ and ± 0.08‰ for $\delta^{13}C$ (1σ).

Powdered shell samples sent to the Institute of Geosciences at the University of Mainz were measured on a Thermo Finnigan MAT 253 continuous-flow isotope ratio mass spectrometer equipped with a Gasbench II. Samples were dissolved with 99.9% phosphoric acid in He-flushed borosilicate exetainers at 72 °C. Data were calibrated against NBS-19 ($\delta^{18}O$ = −2.20‰; $\delta^{13}C$ = +1.95‰) calibrated Carrara marble distributed by IVA Analysentechnik GmbH & Co. KG (Meerbusch, Germany) ($\delta^{18}O$ = −1.90‰; $\delta^{13}C$ = +2.01‰). On average, internal precision (1σ) was ± 0.05‰ for $\delta^{18}O$ and ± 0.04‰ for $\delta^{13}C$. Accuracy is better than 0.06‰ and 0.03‰ for $\delta^{18}O$ and $\delta^{13}C$, respectively, based on 421 blindly measured NBS-19 samples. Isotope ratios of carbonate are reported as per mil (‰) relative to Vienna Pee Dee Belemnite (VPDB).

Stable isotope data of shell carbonate are archived as Supplementary Information.

2.6. Predicted shell $\delta^{18}O$ values

Predicted shell margin $\delta^{18}O$ values based on equilibrium fractionation were calculated using the monthly observations of water temperature and $\delta^{18}O_{water}$ values, and the equilibrium fractionation equation for calcite and water (Friedman and O'Neill, 1977, modified from Tarutani et al., 1969):

$$1000ln\alpha = 2.78 \times 10^6 \times T^{-2} - 2.89 \quad (1)$$

where T is temperature in Kelvin and < is the fractionation factor between calcite and water. The terms < and ™ are related through the equation:

$$\alpha = (\delta_{shell} + 1000)/(\delta_{water} + 1000) \quad (2)$$

where δ values are expressed relative to VSMOW. Temperature estimates based on $\delta^{18}O_{shell}$ values sampled along the axis of maximum growth were calculated assuming a $\delta^{18}O_{water}$ value of −1.22 ± 0.19‰. This value represents the average $\delta^{18}O_{water}$ value and standard deviation during the collection period. Values of $\delta^{18}O_{shell}$ were then reported relative to VPDB using the following equation (Coplen et al., 1983; Gonfiantini et al., 1995):

$$\delta^{18}O_{(VPDB)} = (\delta^{18}O_{(VSMOW)} - 30.91)/1.03091 \quad (3)$$

3. Results

3.1. Mineralogy and microstructure

Acetate peels show four microstructural layers within the shell cross-sections of *N. deaurata* and *N. magellanica* (Fig. 4). These layers are named based on their position relative to the myostracum (layer "m"; the muscle attachment site) following terminology in MacClintock (1967) and Carter and Hall (1990). The microstructural layers ventral to the myostracum are termed m-1 and are composed of calcitic irregularly foliated microstructure. The microstructural layers dorsal to the myostracum are composed of calcitic regularly foliated (m + 1) and irregular simple prismatic (m + 2) microstructure. In both species, Feigl's solution only reveals the presence of aragonite in the myostracum near the apex of the shell, which does not constitute a significant amount of shell material. Therefore, only calcitic components of the shell were sampled for isotopic analyses.

3.2. Shell growth lines

Prominent growth lines are visible in acetate peels and sometimes in polished shell cross-sections, whereas Mutvei's solution revealed both prominent and higher order growth lines. Four of the six shells show three prominent growth lines (ND-1016-1, ND-1016-3, NM-106-3, NM-1016-5), and the remaining two specimens (ND-1016-4 and NM-1016-1) show four prominent growth lines. Occasionally, the presence of a prominent growth line was expressed through to the shell's exterior. Higher order growth lines are spaced between 100 and 200 µm apart and occur in bundles of 10 and 14 micro-growth lines. The time series of $\delta^{18}O_{shell}$ values were used to contextualize the location of prominent growth lines with respect to season of formation and are discussed

Table 1
Collection dates of *Nacella deaurata* and *N. magellanica*, along with SST, salinity, and $\delta^{18}O_{water}$ values relative to VSMOW. Average and standard deviation of temperature, salinity, and $\delta^{18}O_{water}$ values are reported at the bottom of the table.

Date	SST (°C)	$\delta^{18}O_{water}$ (‰)	Salinity (psu)
10/27/15	12.23	−1.28	31.91
11/27/15	11.20	−1.52	30.08
12/31/15	12.23	−1.45	29.46
1/27/16	10.49	−1.16	30.59
2/26/16	12.14	−1.38	30.08
3/29/16	10.58	−1.22	31.21
4/27/16	6.29	−1.35	30.15
5/20/16	5.86	−1.12	31.52
6/23/16	5.06	−0.91	31.42
7/20/16	4.52	−1.02	31.22
9/4/16	5.95	−0.89	30.40
10/1/16	6.89	−0.99	31.29
Average	8.44 ± 3.03	−1.22 ± 0.19	30.73 ± 0.74

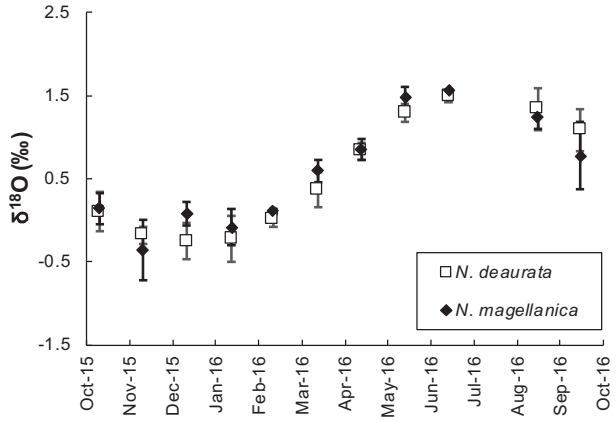

Fig. 6. Monthly shell margin $\delta^{18}O$ values of 33 specimens of *N. deaurata* and *N. magellanica* collected from October 27, 2015 to October 1, 2016. Filled diamonds and open squares represent the mean shell margin $\delta^{18}O$ value (n = 3) for monthly collected specimens of *N. deaurata* and *N. magellanica*, respectively. Error bars represent ± 1 standard deviation from mean $\delta^{18}O$ values.

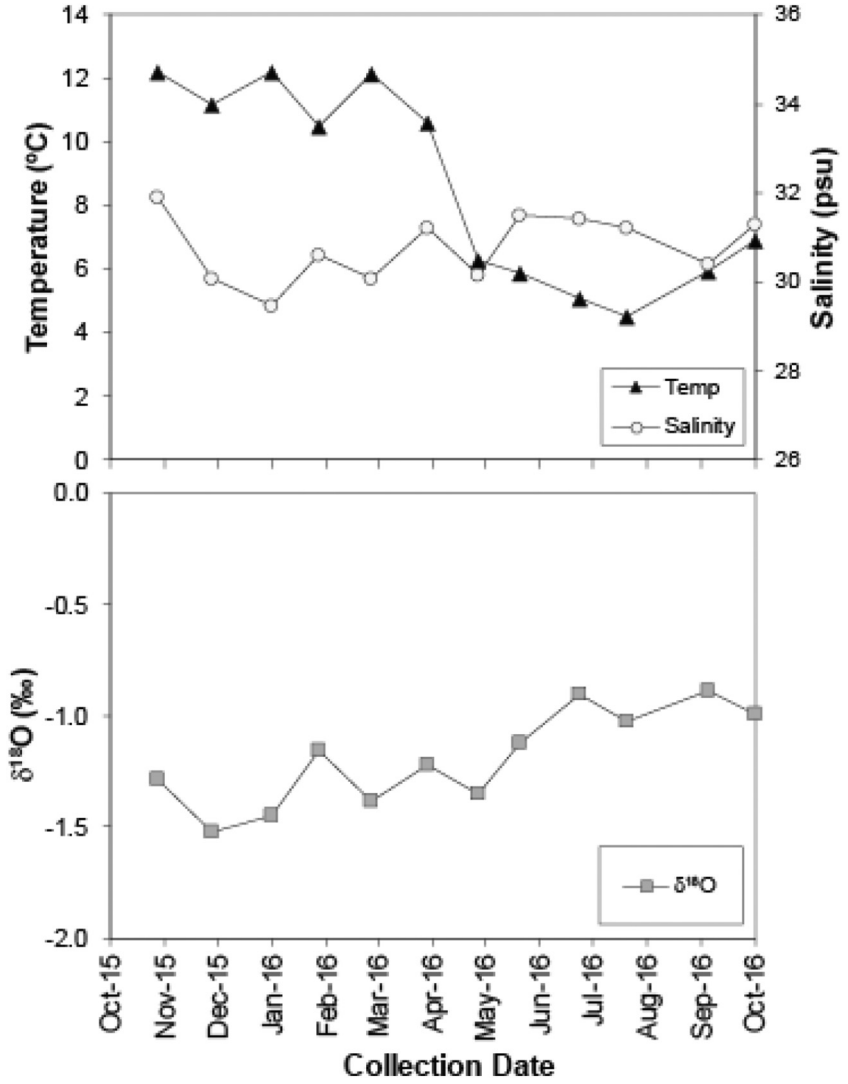

Fig. 5. Time series of water data collected monthly from October 2015 to October 2016. Top panel shows temperature (°C; black triangles) and salinity (psu; white circles). Bottom panel shows $\delta^{18}O_{water}$ values.

below in Section 4.4.

3.3. SST, salinity, and $\delta^{18}O_{water}$ values

Water parameters at the time of monthly limpet collection are listed in Table 1 and shown in Fig. 5. SST ranged from 4.52 to 12.23 °C with an average value of 8.44 ± 3.03 °C. Salinity ranged from 29.46 to 31.91 psu with an average value of 30.73 ± 0.74 psu. Values of $\delta^{18}O_{water}$ ranged from −1.52 to 0.91‰, averaging −1.22 ± 0.19‰.

3.4. Stable isotope ratios of Nacella shells

3.4.1. Monthly shell margin data

Shell margin $\delta^{18}O$ values from specimens collected monthly show a sinusoidal trend reflective of seasonal changes in water temperature (Fig. 6). Average monthly shell margin $\delta^{18}O$ values from *N. deaurata* range from +1.1‰ to +2.8‰. The standard deviation of $\delta^{18}O_{shell}$ values within each monthly collection date is highest in February, September, and October 2016 (± 0.3‰ for each month) and lowest in March and July 2016 (± 0.1‰ for each month). Average monthly $\delta^{18}O_{shell}$ values in *N. magellanica* range from +0.9‰ to +2.9‰. In *N. magellanica*, standard deviation of $\delta^{18}O_{shell}$ values are highest in December 2015 and October 2016 (± 0.4‰ for each month) and lowest in March and July 2016 (within analytical error).

3.4.2. Time series of $\delta^{18}O_{shell}$ and $\delta^{13}C_{shell}$ values

The time series of $\delta^{18}O_{shell}$ values serially sampled along the maximum axis of growth in all six specimens reflect a quasi-sinusoidal trend (Fig. 7). Variation in $\delta^{13}C_{shell}$ values follow a quasi-sinusoidal trend in some shells but not others (Fig. 7). Four of the six shells show $\delta^{13}C_{shell}$ values that are roughly in phase with $\delta^{18}O_{shell}$ values (ND-1016-3, ND-1016-4, NM-1016-3, NM-1016-5). Two of four shells show $\delta^{13}C_{shell}$ values that are out of phase with $\delta^{18}O_{shell}$ values (NM-1016-3, NM-1016-1). Maximum and minimum $\delta^{18}O_{shell}$ and $\delta^{13}C_{shell}$ values for the time series and shell margin data are reported in Table 2.

Values of $\delta^{18}O_{shell}$ and $\delta^{13}C_{shell}$ show no linear correlation, regardless of species or sampling method (i.e., shell margin versus time series) (Fig. 8 and Table 2). In both species, the variance of data points is higher in the shell margin data than in the shells sampled along the maximum axis of growth.

4. Discussion

4.1. Comparison of observed and predicted shell-margin $\delta^{18}O$ values

We compared measured and predicted shell margin $\delta^{18}O$ values to determine whether *N. deaurata* and *N. magellanica* precipitate their shell in isotopic equilibrium with ambient water. Measured shell margin values were offset from predicted values by an average of +1.3 ± 0.4 in *N. deaurata* and by +1.3 ± 0.3‰ in *N. magellanica* (Fig. 9A and B). Although the offset is relatively consistent, and can therefore be accounted for when estimating growth temperature, it is slightly higher in summer months (1.5 ± 0.5‰ for *N. deaurata*; 1.6 ± 0.3‰ for *N. magellanica*) compared to winter months (0.9 ± 0.1‰ for *N. deaurata*; 1.0 ± 0.1‰ for *N. magellanica*). We evaluated the effect of this offset on SST reconstruction in monthly-collected shells by calculating SST using the equilibrium fractionation equation above (Friedman and O'Neill, 1977). Estimated temperatures from $\delta^{18}O_{shell}$ values is lower than observed SST by 5.0 ± 1.6 °C in *N. deaurata* and by 5.2 ± 1.4 °C in *N. magellanica* (Fig. 9C and D). After subtracting 1.3‰ from the measured $\delta^{18}O_{shell}$ values of both species to account for the observed offset, better agreement was reached between calculated and observed temperatures (Fig. 9E and F). Our findings agree with previous studies of patelloid limpets, in which a consistent offset of around +1‰ occurs between observed and predicted $\delta^{18}O_{shell}$ values (Shackleton, 1973; Cohen and Tyson, 1995; Fenger et al., 2007; Ferguson et al., 2011; Colonese et al., 2012; Parker et al., 2017). Despite observing a similar, consistent offset between predicted and observed $\delta^{18}O_{shell}$ values, Colonese et al. (2012) suggested that the two *Nacella* species precipitate their shells in isotopic equilibrium with ambient water. However, the occurrence of an offset from expected equilibrium values indicates that the two *Nacella* species do not form their shells in isotopic equilibrium with ambient water. This difference must be considered in the future to evaluate the analytical possibilities of each species.

4.2. Possible mechanisms of offset from predicted $\delta^{18}O_{shell}$ values

4.2.1. Mineralogy: high vs. low-magnesium calcite

One possible explanation for the positive offset between observed and predicted $\delta^{18}O_{shell}$ values is if calcitic shells are composed of high-magnesium calcite (HMC) rather than low-magnesium calcite (LMC). HMC is defined as calcite in which Mg concentrations are higher than 4 mol-% $MgCO_3$ and typically approach 15 mol-% $MgCO_3$ (Tarutani et al., 1969; Prothero and Schwab, 1996). As shown in Carpenter et al. (1991; their Fig. 5), HMC is ~1‰ more positive than LMC. If calcitic material is composed of HMC, equilibrium fractionation equations require an additional term of 0.06‰ per mol-% $MgCO_3$ (Tarutani et al., 1969; Carpenter et al., 1991). If unaccounted for, this could yield errors in temperature estimates of 0.26 °C per mol-% $MgCO_3$ (Fenger et al., 2007). If the calcitic material is composed of LMC, then no additional terms are required in the equilibrium fractionation equations.

Nacella deaurata and *N. magellanica* would need to contain 22 mol-% $MgCO_3$ to account for the total offset of 1.30‰. Previous work reports that *Patella vulgata* shells (a species within the same family as *Nacella*) are composed of LMC (Fenger et al., 2007). Although we did not measure Mg concentration in the two *Nacella* species, it is reasonable to assume that species within the same family have similar mineralogy, and that the calcitic of portion of *N. deaurata* and *N. magellanica* shells are composed of LMC. Another possible explanation of positive offsets between observed and predicted $\delta^{18}O_{shell}$ values is the occurrence of a vital effect discussed in the next section.

4.2.2. Vital effects

Isotopic disequilibrium can be caused by vital effects, in which an organism's life processes or habits produce isotopic fractionation. Observed departures from equilibrium fractionation are typically negative (e.g., McCrea, 1950; Erez, 1978; Swart, 1983; McConnaughey, 1989a, 1989b; Usdowski and Hoefs, 1993; Spero and Lea, 1996; Spero et al., 1997; Zeebe, 1999; Smith et al., 2000; Adkins et al., 2003), but positive departures from isotopic equilibrium have been observed in benthic algae, foraminifera, non-reef-building corals, barnacles, and marine gastropods (Land et al., 1977; Wefer and Berger, 1980a, 1980b, 1981, 1991; Wefer and Killingley, 1980; Killingley and Newman, 1982; Smith et al., 1988). Schöne et al. (2007) observed no departure from isotopic equilibrium in $\delta^{18}O$ values of intertidal and marine snails from the North Sea, suggesting that isotopic disequilibrium is not attributable to life habit or taxonomic rank. Instead, it seems that isotopic disequilibrium occurs in some species and not in others. Whether an organism precipitates its shell in isotopic disequilibrium may instead depend on processes of shell formation.

In molluscs, shell precipitation occurs in the extrapallial fluid (EPF). The EPF is located in the cavity between the mantle and the shell. Oxygen and carbon are transported to the EPF either through diffusion of CO_2 through the mantle cavity, or through the active transport of CO_3^{2-} and HCO_3^- across the shell's epithelial tissue (Wheeler, 1992). Isotopic disequilibrium may be attributable to kinetic or metabolic isotope effects, which affect the fractionation of heavy isotopes of carbon and oxygen.

Kinetic isotope effects are the result of slower reaction rates of ^{18}O and ^{13}C compared to ^{16}O and ^{12}C, causing preferential incorporation of the lighter isotope into the EPF (McConnaughey, 1989a, 1989b). As such, kinetic isotope effects would cause depletion of ^{18}O and ^{13}C

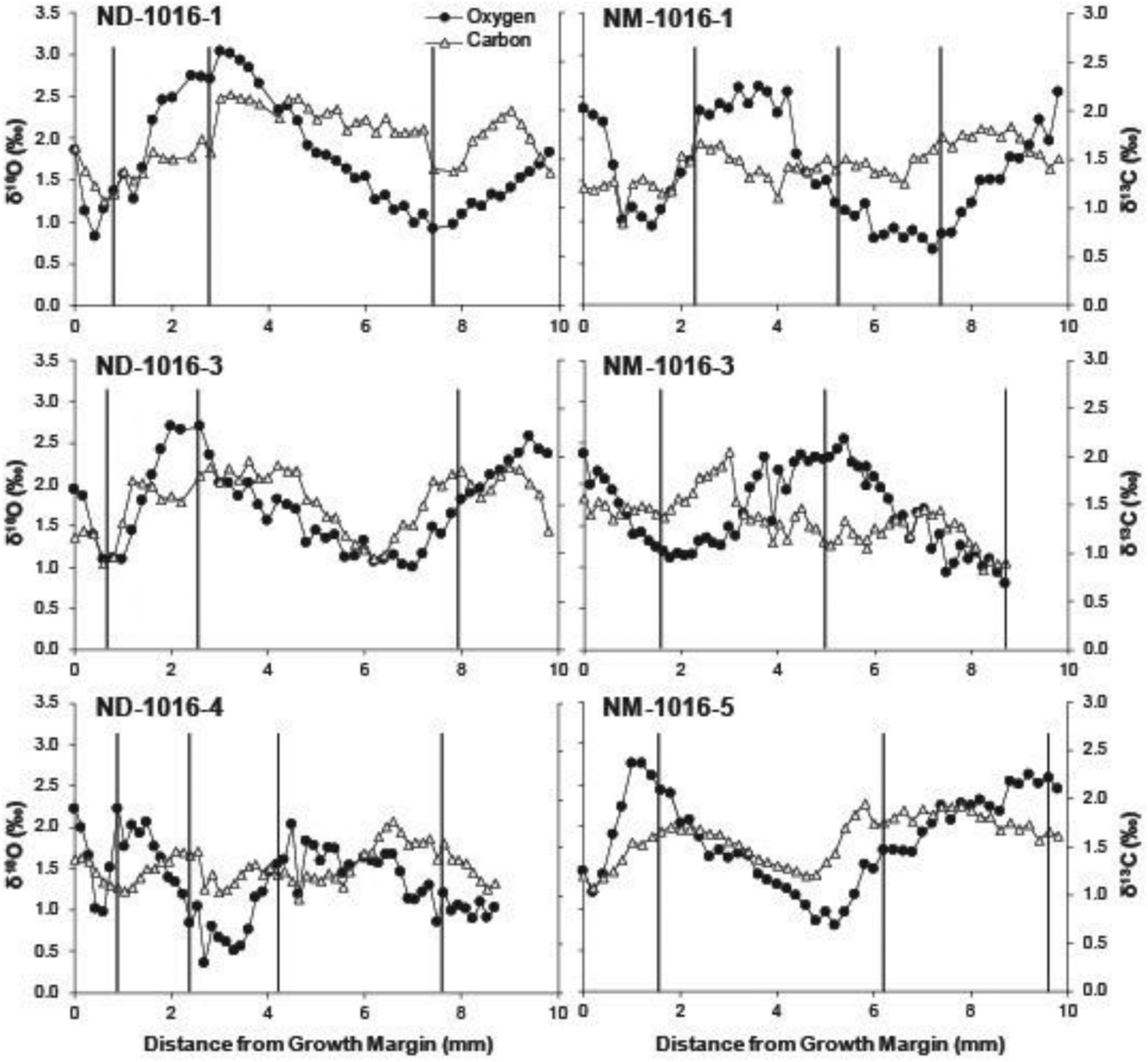

Fig. 7. $\delta^{18}O_{shell}$ and $\delta^{13}C_{shell}$ values of *Nacella deaurata* (left column) and *N. magellanica* (right column) sampled along the axis of maximum growth on the posterior half of the shell. Growth direction is from right to left. Specimen ID is indicated at the top of each time series. Black circles are $\delta^{18}O_{shell}$ values. Gray triangles are $\delta^{13}C_{shell}$ values. Black, vertical lines indicate the location of prominent growth lines. Zero mm from growth margin represents the posterior growth margin.

Table 2
Maximum and minimum $\delta^{18}O_{shell}$ and $\delta^{13}C_{shell}$ values and correlation statistics for time series and shell edge data.

	$\delta^{18}O_{shell}$ (‰)		$\delta^{13}C_{shell}$ (‰)				
Specimen	Minimum	Maximum	Minimum	Maximum	r^2	p-Value	n
N. deaurata							
ND-1016-1	0.4	3.0	1.1	1.9	0.19	0.73	47
ND-1016-3	1.0	2.7	0.9	2.0	0.34	0.01	49
ND-1016-4	0.4	2.2	1.0	1.7	0.01	0.51	58
Shell margins	0.8	2.9	0.3	3.2	0.30	0.10	33
N. magellanica							
NM-1016-1	0.7	2.6	0.9	1.8	0.00	0.10	50
NM-1016-3	0.8	2.5	0.8	2.1	0.00	< 0.01	50
NM-1016-5	0.8	2.8	1.1	1.9	0.23	0.01	50
Shell margins	0.5	2.9	0.6	2.9	0.09	0.67	33

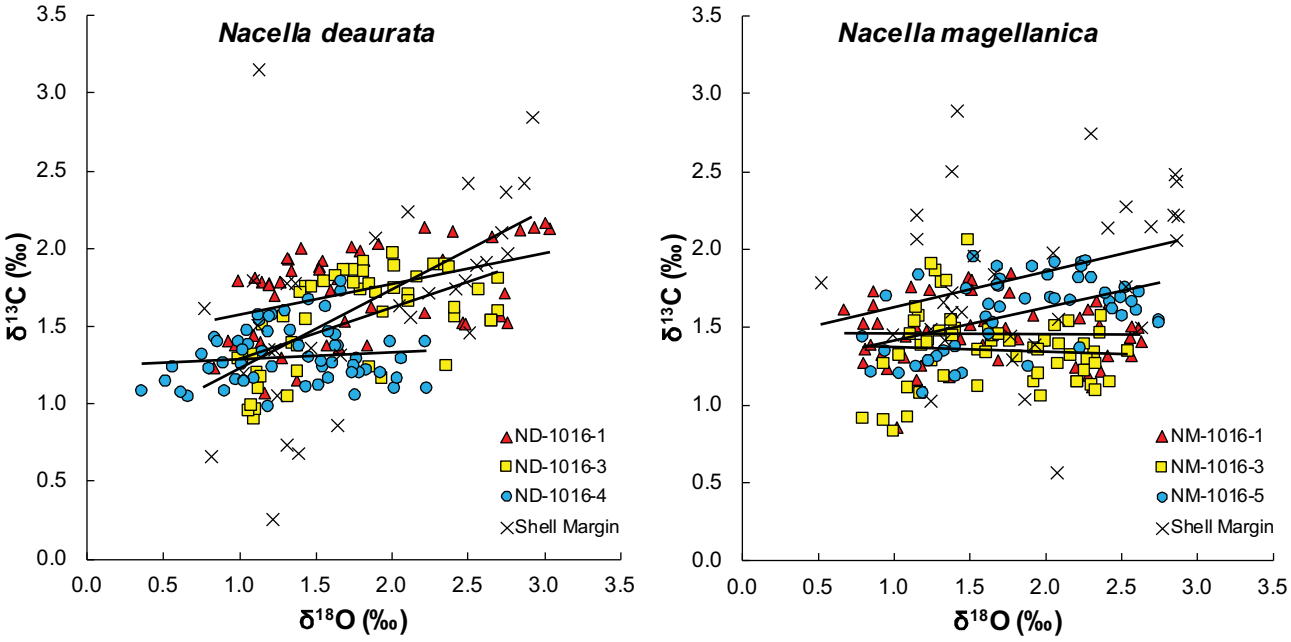

Fig. 8. Cross-plots of $\delta^{18}O$ and $\delta^{13}C$ values of *Nacella deaurata* (left), and *N. magellanica* (right). Colored triangles, squares, and circles represent individual specimens sampled along the maximum axis of growth. Black crosses represent monthly values sampled along the anterior growth margin. (For interpretation of the references to color in this figure legend, the reader is referred to the web version of this article.)

relative to expected equilibrium values (Erez, 1978; McConnaughey, 1989b). Covariation between $\delta^{18}O$ and $\delta^{13}C$ values would be expected in materials affected by kinetic isotope effects. However, no such covariation is observed in either *Nacella* species, regardless of sampling method (Fig. 7). These results are consistent with previous studies of patelloid limpets by Fenger et al. (2007). Therefore, we conclude that kinetic isotope effects are minimal in *Nacella* shells.

Metabolic isotope effects may explain departures from isotopic equilibrium during shell formation. Metabolic isotope effects include incorporation of respired CO_2 or changes in the pH of the biomineralization medium (Swart, 1983; McConnaughey, 1989b). However, metabolic isotope effects typically produce *negative* departures from isotopic equilibrium, in which observed $\delta^{18}O$ values are *lower* than predicted values (e.g., McCrea, 1950; Erez, 1978; Swart, 1983; McConnaughey, 1989a, 1989b; Usdowski and Hoefs, 1993; Spero and Lea, 1996; Spero et al., 1997; Zeebe, 1999; Smith et al., 2000; Adkins et al., 2003). Other studies have investigated whether positive departures from isotopic equilibrium can be attributed to external factors affecting the isotopic composition of the ambient water.

Enrichment of ^{18}O in shell carbonate relative to isotopic equilibrium may occur through enhanced evaporative conditions of the ambient water, such as in tide pools. Schifano and Censi (1983) attributed ^{18}O enrichment in *Patella coerulea* shells to enhanced evaporative conditions during the time of shell precipitation. However, a later study by Schifano and Censi (1986) observed similar enrichment in ^{18}O in *P. coerulea* inhabiting the subtidal zone. Thus, enhanced evaporation does not explain the positive offset from isotopic equilibrium in this species. Moreover, *N. deaurata* and *N. magellanica* do not inhabit microhabitats strongly influenced by evaporation (i.e., tidal pools). Furthermore, ^{18}O enrichment due to evaporation would likely vary throughout the year and, as such, would produce a variable offset between observed and predicted $\delta^{18}O_{shell}$ values. Because we observe a consistent offset, evaporation is not a reasonable explanation for positive departures from isotopic equilibrium in *N. deaurata* and *N. magellanica*.

Internal processes of the organism may also cause enrichment of ^{18}O relative to equilibrium, resulting in a positive offset between observed and predicted $\delta^{18}O_{shell}$ values. Land et al. (1977) explained positive departures in $\delta^{18}O_{shell}$ values relative to equilibrium in non-reef-building corals resulting from the transport of ^{16}O out of the biomineralization medium (i.e., an internal, vital process). A similar process may occur in the EPF of *N. deaurata* and *N. magellanica*. Alternatively, McConnaughey (1989a) attributed enrichment of ^{18}O in barnacles relative to equilibrium through some unknown internal process affecting biomineralization.

The cause of observed offsets between observed and predicted $\delta^{18}O_{shell}$ values in *N. deaurata* and *N. magellanica* merits further study. Observation of *N. deaurata* and *N. magellanica* under laboratory conditions may provide further insight. The calibration of these two species as SST archives will be further refined by comparing the high-resolution $\delta^{18}O_{shell}$ time series to higher resolution SST measurements. Efforts are underway to acquire a higher resolution SST record at the study site. Although *N. deaurata* and *N. magellanica* form their shells in isotopic disequilibrium, departures from equilibrium are predictable and consistent, allowing for reliable reconstruction of SST after taking the observed offsets into account.

4.3. Ontogenetic variation in $\delta^{18}O_{shell}$ time series

We compared $\delta^{18}O_{shell}$ values sampled along the maximum axis of growth (i.e., high-resolution isotopic time series) among individuals and between species to determine whether *N. deaurata* and *N. magellanica* record similar ontogenetic variation. Both species show reasonable agreement in the amplitudes of the $\delta^{18}O_{shell}$ time series (Fig. 7). ND-1016-1 records a higher-than-average maximum $\delta^{18}O_{shell}$ value of 3.03‰ (average maximum $\delta^{18}O_{shell}$ is 2.65 ± 0.26‰). This higher-than-average maximum $\delta^{18}O_{shell}$ value occurs within the last year of shell growth but yields temperature estimates which still fall within one standard deviation of observed temperatures during the collection period. ND-1016-4 records a lower-than-average minimum $\delta^{18}O_{shell}$ value of 0.36‰ (average minimum $\delta^{18}O_{shell}$ is 0.74 ± 0.22‰). This lower-than average minimum $\delta^{18}O_{shell}$ value occurs after the first year of growth and falls outside of the range of observed temperatures during the collection period (Fig. 7, see Section 4.4 for a discussion of temperature estimates). General agreement is also observed between $\delta^{18}O_{shell}$ values at the posterior growth margin of shells sampled along the maximum axis of growth. Average $\delta^{18}O_{shell}$ values at the posterior

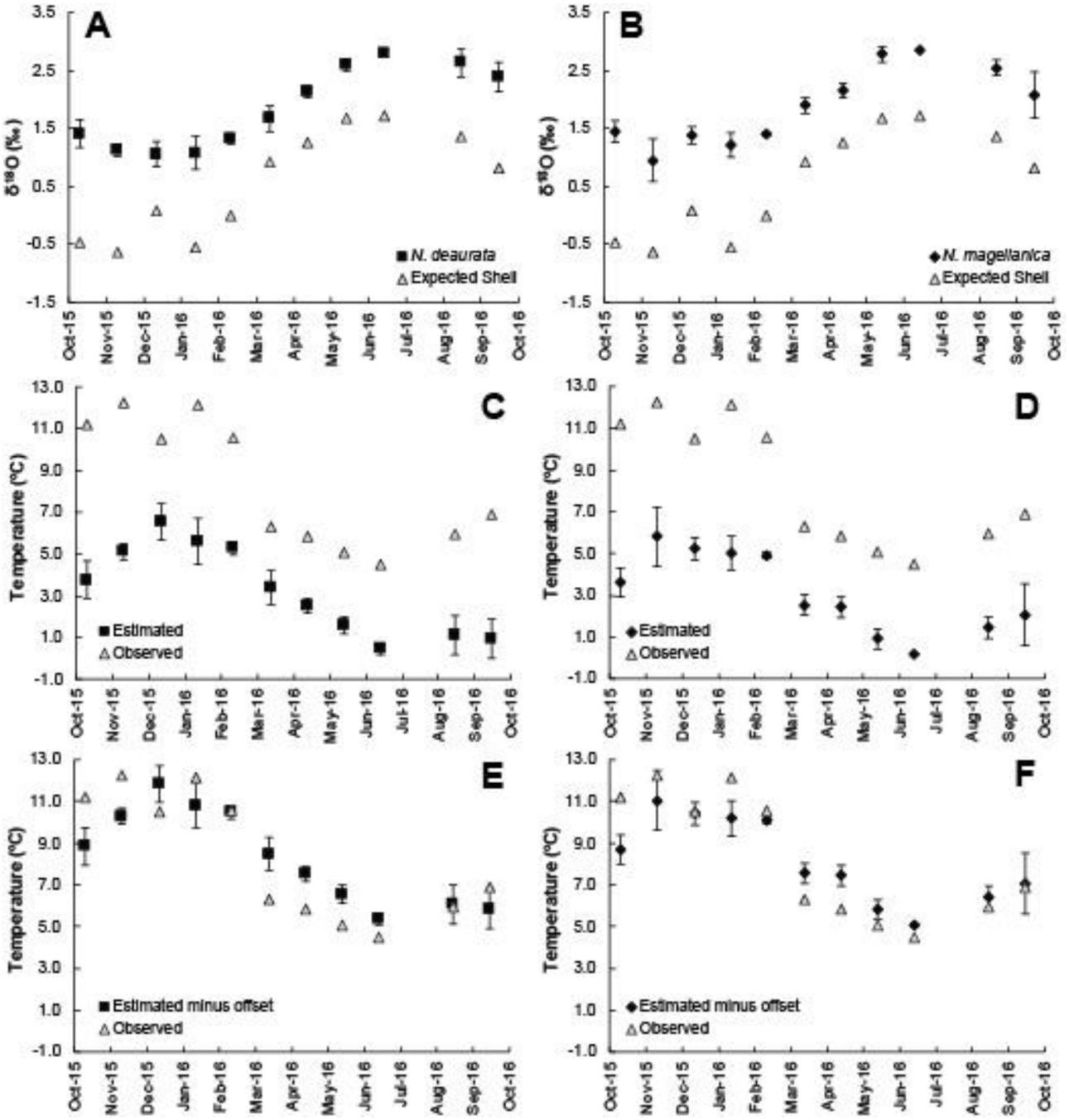

Fig. 9. The effect of positive offset from expected oxygen isotope equilibrium on estimated SST (*N. deaurata* left panels; *N. magellanica* right panels). A) *N. deaurata*: Shell margin $\delta^{18}O$ values before accounting for the consistent offset of $+1.3 \pm 0.4$‰. B) *N. magellanica*: Shell margin $\delta^{18}O$ values before accounting for the consistent offset of $+1.3 \pm 0.3$‰. C) Comparison of observed and estimated SST directly from measured $\delta^{18}O$ values in *N. deaurata* shell margins. D) Comparison of observed and estimated SST directly from measured $\delta^{18}O$ values in *N. magellanica* shell margins. D) Comparison of observed SST and corrected estimated SST (subtracting 1.3‰ from $\delta^{18}O$ values of *N. deaurata* shell margins. E) Comparison of observed SST and corrected estimated SST (subtracting 1.3‰ from $\delta^{18}O$ values of *N. magellanica* shell margins). Error bars represent 1 standard deviation from the mean ($n = 3$). Gray triangles represent expected $\delta^{18}O_{shell}$ values (top panels) and observed temperatures (middle and bottoms).

margin of growth in these shells is 2.03 ± 0.36‰. SST estimated using this average is 7.54 ± 1.40 °C, which is within one standard deviation of observed temperature at the time of shell collection in October 2016 (6.89 °C).

One shell (specimen NM-1016-5) records a $\delta^{18}O_{shell}$ value at its posterior margin that falls outside of one standard deviation from mean values (1.45‰). We considered several possible explanations for this difference. All shells measured for $\delta^{18}O_{shell}$ values along the maximum axis of growth were sampled on the same collection date (October 1st, 2016), and from the same location along the shore. Therefore, it is unlikely that variation in temperature or oxygen isotope ratios of water would explain the difference in posterior-growth-margin $\delta^{18}O_{shell}$ values between NM-1016-5 and the other shells in this study. A damaged shell margin could result in a lack of preservation of the last increment of growth prior to harvest. Inspection of the posterior shell margin of specimen NM-1016-5 showed no such damage. Previous studies have shown that slower growth rates associated with senescence later in ontogeny can produce increased time averaging, and hence, truncated

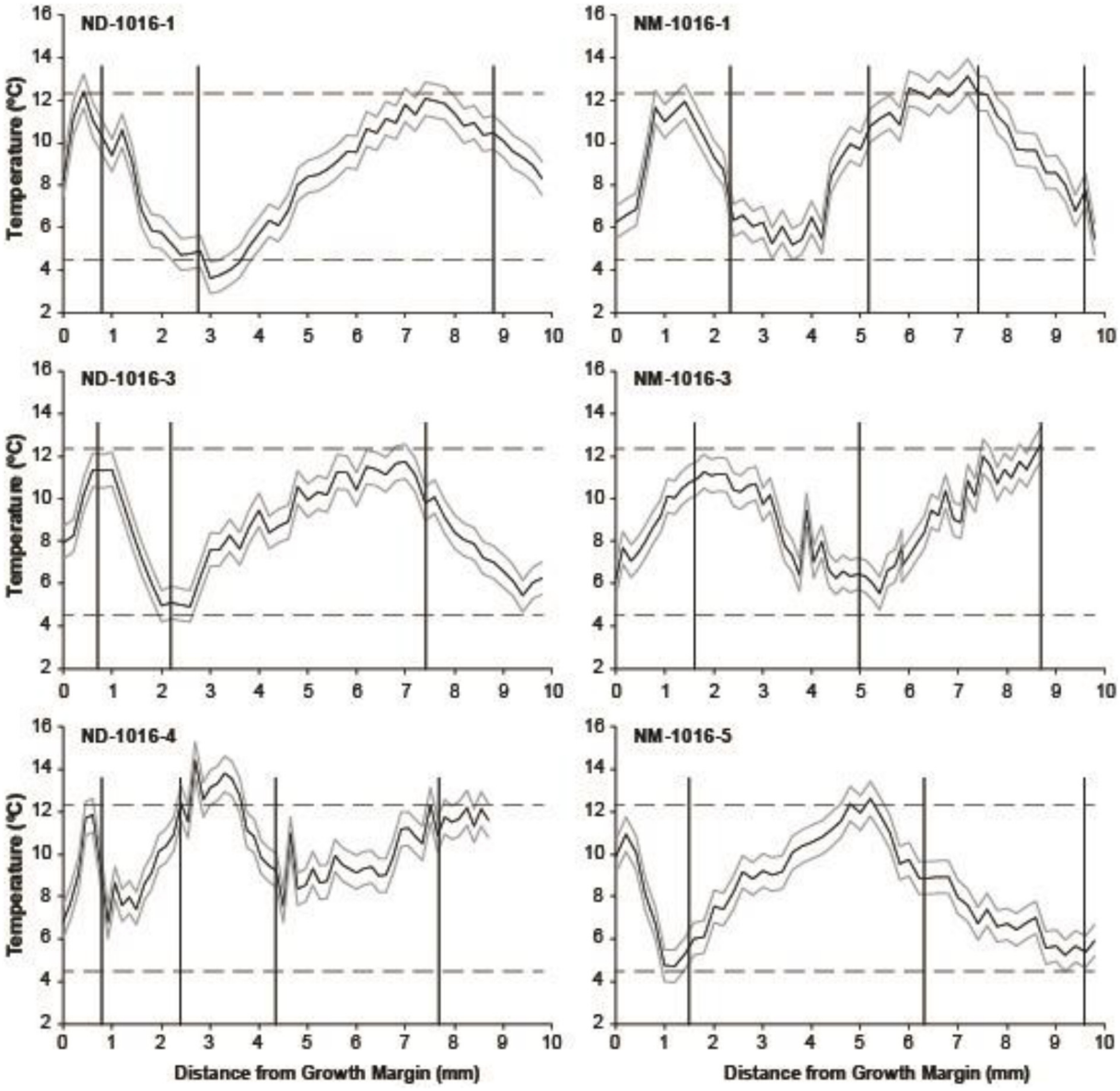

Fig. 10. Temperature estimates derived from $\delta^{18}O_{shell}$ time series of each of the six specimens sampled along the maximum axis of growth. We subtracted 1.3‰ from measured $\delta^{18}O_{shell}$ values prior to calculating temperature to account for the positive offset from isotopic equilibrium. The black line represents estimated temperatures assuming $\delta^{18}O_{water}$ values of −1.22‰, the mean $\delta^{18}O_{water}$ value during the calibration period. Gray lines represent temperature estimates made using ± 1 standard deviation from mean water $\delta^{18}O$ values (± 0.19‰). Black, vertical lines represent the location of prominent growth lines. Horizontal, dashed lines represent maximum and minimum SST observed from October 27, 2015 to October 1, 2016.

records (e.g.: Jones et al., 1986; Weidman et al., 1994; Goodwin et al., 2003; Surge and Walker, 2006; Fenger et al., 2007). Specimen NM-1016-5 displays a high frequency sinusoidal pattern toward the growth margin, suggesting a slower growth rate during the last year of life (see Section 4.6). Therefore, we attribute differences in $\delta^{18}O_{shell}$ values at the posterior growth margin of shell in NM-1016-5 relative to that of the other specimens to time averaging associated with slowed growth at senescence. This finding emphasizes the importance high-resolution micro-sampling of several individuals to obtain the most complete record of variation.

To test agreement between reconstructed and observed SST time series, we calculated temperature using the equilibrium fractionation equation (Friedman and O'Neill, 1977) after subtracting 1.30‰ from measured $\delta^{18}O_{shell}$ values to account for the observed offset from equilibrium values and assuming a $\delta^{18}O_{water}$ value of -1.22 ± 0.09‰ (the average and standard deviation of $\delta^{18}O_{water}$ values from the shell collection period) (Fig. 10). With the exception of ND-1016-4, all shells capture maximum and minimum SST observed during the collection period in the last year of shell growth. Shell NM-1016-4 does not capture minimum winter SST in its last year of growth, which we attribute to increased time-averaging due to senescence. However, estimates of SST in the last year of growth all fall within the range of observed SST during the collection period, suggesting that SST reconstructions using $\delta^{18}O_{shell}$ time series are reliable after accounting for the observed offset.

4.4. Timing of prominent growth line formation

Previous studies of shell growth have documented prominent growth lines that form annually in response to maximum or minimum growth temperature thresholds, reproductive processes, or seasonal food supply (e.g., Pannella and MacClintock, 1968; Lutz and Rhoads, 1977; Jones, 1983; Arthur and Allard, 1987; Jones et al., 1989, 1990; Cerrato et al., 1991; Jones and Quitmyer, 1996; Surge et al., 2001; Schöne et al., 2005b; Fenger et al., 2007; García-March et al., 2011;

Surge et al., 2013). Based on the seasonal timing estimated from the reconstructed SST time series, prominent growth lines in *N. deaurata* and *N. magellanica* do not form once annually (Fig. 10). Instead, they form roughly twice per year. Prominent growth lines in the two *Nacella* species occur at or near maximum and minimum $\delta^{18}O_{shell}$ values, which would imply slowed growth or cessation during both summer and winter. One shell (specimen NM-1016-1) shows a prominent growth line that formed between summer and winter. Prominent growth lines coincident with maximum $\delta^{18}O_{shell}$ values (i.e., winter) may result from growth slowdown or cessation due to cold temperature thresholds. The lower number of $\delta^{18}O_{shell}$ measurements (i.e., data points) at or near maximum $\delta^{18}O_{shell}$ values implies that less material is accreted during colder conditions. Previous studies of patelloid limpets from mid to high latitudes have shown similar growth slowdown or cessation in winter (e.g. Blackmore, 1969; Lewis and Bowman, 1975; Ekaratne and Crisp, 1984; Jenkins and Hartnoll, 2001; Fenger et al., 2007; Surge et al., 2013). Given our observations, temperature thresholds alone cannot explain the timing of prominent growth line formation.

Another possible explanation for the formation of prominent growth lines is growth slowdown or cessation due to seasonal changes in food supply. Variation in $\delta^{13}C_{shell}$ values can potentially be used to test whether food supply influences the formation of prominent growth lines. Seasonal variation in $\delta^{13}C_{shell}$ values has been linked to changes in primary productivity and respiration (i.e., the decomposition of organic matter) (Arthur et al., 1983; Krantz et al., 1987; Hickson et al., 1999; Schöne et al., 2005b). Primary production preferentially uses the lighter isotope, causing an enrichment in ^{13}C of the surrounding carbon reservoirs. Conversely, respiration releases ^{12}C into surrounding carbon reservoirs. Therefore, high $\delta^{13}C_{shell}$ values may indicate higher primary productivity, and low $\delta^{13}C_{shell}$ values may represent periods of increased respiration. If food supply controls shell growth, then faster growth would coincide with higher primary productivity, and slower growth would coincide with lower primary productivity (Surge et al., 2013). Consequently, prominent growth lines should form in conjunction with minimum $\delta^{13}C_{shell}$ values. This can be seen in summer of the last year of growth in ND-1016-1, ND-1016-3, and ND-1016-4, and in the winter in NM-1016-3 (around 5 mm from the growth margin). Seasonal changes in food supply could then explain prominent growth line formation in summer months, particularly in *N. deaurata*. However, it is difficult to determine whether primary productivity influences seasonal variation in $\delta^{13}C_{shell}$ values, as this study lacks the records of water parameters necessary to calculate expected $\delta^{13}C_{shell}$ values (see Section 4.7).

Other studies have suggested that reproductive stress may produce growth slowdown or cessation in molluscs (e.g. Pannella and MacClintock, 1968; Ekaratne and Crisp, 1984; Surge et al., 2013). Spawning in *N. deaurata* and *N. magellanica* can occur any time after August, as temperatures begins to rise, with a peak spawning event occurring the late spring (November/December) (Morriconi, 1999; Morriconi, 2005). Therefore, prominent growth lines observed at or near minimum or intermediate $\delta^{18}O_{shell}$ values (summer and spring/autumn, respectively) may have formed as a result of slowed growth due to reproductive stress. The cause of prominent growth line formation in *N. deaurata* and *N. magellanica* remains unclear, but prominent growth line formation does not seem to occur once annually in either species and, therefore, they cannot be used as annual growth checks to estimate ontogenetic age.

4.5. Minor growth increments

Colonese et al. (2012) suggested that prominent growth lines in *N. deaurata* and *N. magellanica* occur at fortnightly intervals. We observe similar fortnightly growth increments in *N. deaurata* and *N. magellanica* (Fig. 1C); however, they are distinct from the prominent growth lines described in Section 4.4 above and more likely represent higher order growth features. These minor growth increments occur in bundles of 10–14 micro-growth increments and likely represent fortnightly growth due to diurnal tidal frequency. Previous studies have observed similar fortnightly tidal bundles of minor growth increments in limpets (Ekaratne and Crisp, 1982, 1984; Fenger et al., 2007; Colonese et al., 2012). Fenger et al. (2007) attributed the formation of fortnightly increments to changes in food abundance associated with tidal oscillation. Because *N. deaurata* and *N. magellanica* primarily source their diets from the low and middle intertidal zone (Rosenfeld et al., 2018), it is possible that tidal growth is achieved through changes in food availability as the intertidal zone is submerged and exposed.

4.6. Lifespans and growth rates

Although prominent growth lines in *N. deaurata* and *N. magellanica* do not form annual growth checks and cannot be reliably used to estimate ontogenetic age, lifespans can be inferred using the seasonal variation in $\delta^{18}O_{shell}$ time series. Based on observed seasonal cycles of $\delta^{18}O_{shell}$ variation, *N. deaurata* and *N. magellanica* show observable lifespans of 2–3 years. However, because the apex of each species contains aragonite and was avoided during micromilling for isotopic analyses, lifespan is underestimated probably by several months. Previous studies of patelloid limpets at northern mid latitudes have observed 5–9 annual cycles in $\delta^{18}O_{shell}$ values (Fenger et al., 2007; Surge et al., 2013). *Nacella deaurata* and *N. magellanica* have shorter lifespans and grow more slowly than other patelloid limpets. Moss et al. (2016) report that slower growth rates in bivalves may result from cold temperature thresholds at higher latitudes, but that lifespans tend to increase at higher latitudes. *Nacella* spp. occupy the cold-temperate region (as defined by Briggs and Bowen, 2012) along the southern tip of South America, but show faster growth and shorter lifespans than other patelloid limpets from cold-temperate regions (e.g., *Patella vulgata*: Fenger et al., 2007). Thus, *Nacella* spp. do not follow the expected pattern found in marine bivalves by Moss et al. (2016).

Colonese et al. (2012) report an average growth rate of 18 mm/yr in one year of growth in one specimen of *N. deaurata* and average growth rates of 9 mm/yr and 13 mm/yr in the last two years of growth in one specimen of *N. magellanica*. In a larger sample size, we observed generally slower growth rates, particularly in the third year of shell growth. Specimens ND-1016-1, ND-1016-3, and NM-1016-1 show growth rates of ~7 mm/yr in their first year of growth and a growth rate of ~4 mm/yr in their second year of growth. Specimen NM1016-3 shows annual growth rates of ~4 mm/yr in their second year of growth. NM-1016-5 shows a growth rate of ~2 mm/yr in its second year of growth, and a growth rate of ~8 mm/yr in its first year of growth. ND-1016-4 shows a growth rate of ~3 mm/yr in its second year of growth, and a growth rate of ~1 mm/yr in its third year of growth. Growth rates during the first year of shell growth are difficult to determine in shells ND-1016-4 and NM-1016-3 as records of the first year of growth are truncated due to the aragonitic portion of the shell not being sampled. Previous work by Colonese et al. (2012) only examined one individual of each species showing only 1–2 years of growth; therefore, our findings illustrate the need for a larger sample size when attempting to determine growth rate and lifespan.

4.7. Variability in $\delta^{13}C_{shell}$ values

Values of $\delta^{13}C_{shell}$ are more difficult to interpret than $\delta^{18}O_{shell}$ values due to the lack of relevant water parameters necessary for reconstructing expected $\delta^{13}C_{shell}$ values (e.g., chlorophyll, $\delta^{13}C$ of dissolved inorganic carbon (DIC)). Variation in $\delta^{13}C_{shell}$ values appear to follow similar cyclical trends as $\delta^{18}O_{shell}$ values in half of observed specimens (ND-1016-1, ND-1016-3, NM-1016-5; Fig. 7). This finding suggests some seasonal influence on $\delta^{13}C_{shell}$ values in some shells, but not in others. Some studies have shown a correspondence between salinity and $\delta^{13}C_{shell}$ values (Surge et al., 2001; Fry, 2002). For example, values of $\delta^{13}C_{shell}$ may relate to $\delta^{13}C_{DIC}$ through the activity of the

enzyme carbonic anhydrase, which has shown changes with increasing salinity in some bivalves (Henry and Saintsing, 1983; Gillikin et al., 2010). However, salinity at the study site is relatively constant throughout the year, and, therefore, cannot explain seasonal $\delta^{13}C_{shell}$ variations seen here. Furthermore, we do not observe large negative excursions in $\delta^{18}O_{shell}$ values that may result from the influx of freshwater from snowmelt. It is also possible that variation in $\delta^{13}C_{shell}$ is linked to changes in $\delta^{13}C_{DIC}$ through changes in primary productivity (see Section 4.4). However, without records of relevant water parameters, controls on the $\delta^{13}C_{shell}$ values of *N. deaurata* and *N. magellanica* remain a topic of further study.

5. Conclusions

Nacella deaurata and *N. magellanica* do not precipitate their shells in isotopic equilibrium with ambient seawater. Instead, $\delta^{18}O_{shell}$ values observed in shells are offset from expected equilibrium $\delta^{18}O_{shell}$ values by 1.28 ± 0.39‰ (*N. deaurata*) and 1.32 ± 0.32‰ (*N. magellanica*). These offsets are consistent throughout the shell collection period and can therefore be subtracted from observed $\delta^{18}O_{shell}$ values to yield reliable estimates of growth temperature. SST calculated from $\delta^{18}O_{shell}$ values showed agreement with monthly in situ measurements of SST after accounting for this offset. Isotopic disequilibrium is likely not caused by kinetic or metabolic isotope effects, or by external factors such as evaporation or changes in pH of seawater. It is more likely that the observed offset results from an internal, vital process of the organism. Observation of both species under controlled conditions may provide insight into the cause of observed offsets between predicted and observed $\delta^{18}O_{shell}$ values. The magnitude of this offset could be further refined with higher resolution SST measurements over a longer monitoring period. Prominent growth lines do not form once annually in either species and, therefore, cannot be used as annual growth checks to estimate ontogenetic age. Instead, prominent growth lines form approximately twice annually at or near maximum and minimum $\delta^{18}O_{shell}$ values (i.e. in summer and winter). Prominent growth lines formed in winter are most likely the result of slowed growth due to colder temperatures, whereas prominent lines formed in summer are most likely due to slowed growth due to reproductive stress. Observation of the growth of the two species under laboratory conditions could reveal the cause of formation of prominent growth lines. Minor growth increments occur in bundles of 10–14 micro-growth lines, likely representing periods of growth due to diurnal tidal influences. The rich archaeological deposits in this region date to important climate episodes during the late Holocene, such as the Medieval Climate Anomaly and Little Ice Age (Álvarez et al., 2018). Thus, our future isotopic analysis of archaeological *Nacella* specimens will potentially provide much needed information about Holocene seasonality at sub-monthly resolution from high-latitude South American locations. Moreover, the archaeological context of such data can provide information on human behavior and ultimately human-climate interactions.

Declaration of competing interest

The authors declare that they have no known competing financial interests or personal relationships that could have appeared to influence the work reported in this paper.

Acknowledgements

Thanks to Lauren Graniero and David Moss for perspectives on interpreting data. Thanks to Joe Carter, Andy Johnson, Laurie Steponaitis, John Bane, Larry Benninger, and Joel Hudley for comments and discussions on this work. Kylie Palmer helped with calculating *p*-values in Table 2. Special thanks to David Dettman at the University of Arizona for performing stable isotope analyses. Comments from two anonymous reviewers improved the quality of this paper. Funding for this project was provided by: the United States National Science Foundation (NSF) (project OCE-1803311; awarded to DS); the Preston Jones and Mary Elizabeth Frances Dean Martin Fellowship Fund at the University of North Carolina at Chapel Hill, Department of Geological Sciences to AN; projects PIP-0706 (CONICET), PICT2148 (MINCyT) funded by the Argentinean Federal Government; project HAR2009-06996 funded by the Spanish Ministry of Science and Innovation; and Project GR-7846 funded by the Wenner-Gren Foundation of Anthropological Research (USA). Maria Bas has participated in this work with the support of a doctoral fellowship funded by CONICET for the completion of a PhD in Biological Sciences at Universidad Nacional de Mar del Plata (Argentina).

References

Adkins, J., Boyle, E., Curry, W., Lutringer, A., 2003. Stable isotopes in deep-sea corals and a new mechanism for "vital effects". Geochim. Cosmochim. Acta 67, 1129–1143.
Álvarez, M., Briz i Godino, I., Pal, N., Bas, M., Lacrouts, A., 2018. Climatic change and human-marine interactions in the uttermost tip of South America in Late Holocene. Quat. Int.
Ambrose Jr., W., Locke, W., Bigelow, G., Renaud, P., 2016. Deposition of annual growth lines in the apex of the common limpet (*Patella vulgata*) from Shetland Islands, UK and Norway: evidence from field marking and shell mineral content of annual line deposition. Environ. Archaeol. 21, 79–87.
Arthur, M., Allard, D., 1987. Unlocking the mysteries of *Mercenaria*. Maritimes 31, 14–17.
Arthur, M., Williams, F., Jones, D., 1983. Seasonal temperature-salinity changes and thermocline development in the mid-Atlantic Bight as recorded by the isotopic composition of bivalves. Geology 11, 655–659.
Blackmore, D., 1969. Studies of *Patella vulgata* LI in growth, reproduction, and zonal distribution. J. Mar. Exp. Biol. Ecol. 3, 200–213.
Borromei, A.M., Quattrocchio, M., 2001. Palynological study of Holocene marine sediments from Bahía Lapataia, Beagle Channel, Tierra del Fuego, Argentina. Rev. Esp. Micropaleontol. 33, 61–70.
Borromei, A.M., Coronato, A., Franzén, L.G., Ponce, J.F., Sáez, J.A.L., Maidana, N., Rabassa, J., Candel, M.S., 2010. Multiproxy record of Holocene paleoenvironmental change, Tierra del Fuego, Argentina. Palaeogeogr. Palaeoclimatol. Palaeoecol. 286, 1–16.
Briggs, J., Bowen, B., 2012. A realignment of marine biogeographic provinces with particular reference to fish distributions. J. Biogeogr. 39, 12–30.
Candel, M.S., Borromei, A.M., Martínez, M.A., Gordillo, S., Quattrocchio, M., Rabassa, J., 2009. Middle–Late Holocene palynology and marine mollusks from Archipiélago Cormoranes area, Beagle Channel, southern Tierra del Fuego, Argentina. Palaeogeogr. Palaeoclimatol. Palaeoecol. 273, 111–122.
Carpenter, S., Lohmann, K., Holden, P., Walter, L., Huston, T., Halliday, A., 1991. $\delta^{18}O$ values, $^{87}Sr/^{86}Sr$ and Sr/Mg ratios of Late Devonian abiotic calcite: implications for the composition of ancient seawater. Geochim. Cosmochim. Acta 55, 1991–2010.
Carter, J., Ambrose, W., 1989. Techniques for studying molluscan shell microstructure. The Paleontological Society Special Publications 4, 101–119.
Carter, J., Hall, R., 1990. Polyplacophora, Scaphopoda, Archaeogastropoda and Paragastropoda (Mollusca). In: Carter, J.G. (Ed.), Skeletal Biomineralization: Patterns, Processes and Evolutionary Trends, Vol. 2. Van Nostrand Reinhold, Hoboken, N. J, pp. 29–51.
Cerrato, R., Wallace, H., Lightfoot, K., 1991. Tidal and seasonal patterns in the chondrophore of the soft shell clam *Mya arenaria*. Biol. Bull. (Woods Hole) 181, 307–311.
Cohen, A., Tyson, P., 1995. Sea-surface temperature fluctuations during the Holocene off the south coast of Africa: Implications for terrestrial climate and rainfall. Holocene 5, 304–312.
Colonese, A., Verdún-Castelló, E., Álvarez, M., Godino, I., Zurro, D., Salvatelli, L., 2012. Oxygen isotopic composition of limpet shells from the Beagle Channel: implications for seasonal studies in shell middens of Tierra del Fuego. J. Archaeol. Sci. 39 (6), 1738–1748.
Coplen, T., Kendall, C., Hopple, J., 1983. Comparison of stable isotope reference samples. Nature 306, 236–238.
Craig, H., 1957. Isotopic standards for carbon and oxygen and correction factors for mass-spectrometric analysis of carbon dioxide. Geochim. Cosmochim. Acta 12, 133–149.
Dätwyler, C., Neukom, R., Abram, N.J., Gallant, A.J., Grosjean, M., Jacques-Coper, M., 2018. Teleconnection stationarity, variability and trends of the Southern Annular 660 Mode (SAM) during the last millennium. Clim. Dyn. 51 (661), 2321–2339.
Ekaratne, S., Crisp, D., 1982. Tidal micro-growth bands in intertidal gastropod shells, with an evaluation of band-dating techniques. Proc. R. Soc. London, Ser. B 214, 305–323.
Ekaratne, S., Crisp, D., 1984. Seasonal growth studies of intertidal gastropods from shell micro-growth band measurements, including a comparison with alternative methods. J. Mar. Biol. Assoc. UK 64, 13–210.
Epstein, S., Buchsbaum, R., Lowenstam, H., Urey, H., 1951. Carbonate-water isotopic temperature scale. Geol. Soc. Am. Bull. 62, 417–425.
Epstein, S., Buchsbaum, R., Lowenstam, H., Urey, H., 1953. Revised carbonate-water isotopic temperature scale. Geol. Soc. Am. Bull. 64, 1315–1326.
Erez, J., 1978. Vital effect on stable-isotope composition seen in foraminifera and coral skeletons. Nature 273, 199–202.
Estevez, J., Pianab, E., Schiavinib, A., Juan-Muns, N., 2001. Archaeological analysis of

shell middens in the beagle channel, Tierra Del Fuego Island. Int. J. Osteoarchaeol. 11, 24–33.
Feigl, F., 1958. Spot Tests in Inorganic Analysis, 5th ed. Elsevier, New York, pp. 469–470.
Fenger, T., Surge, D., Schöne, B., Milner, N., 2007. Sclerochronology and geochemical variation in limpet shells (*Patella vulgata*): a new archive to reconstruct coastal sea surface temperature. Geochem. Geophys. Geosyst. 8, Q07001. https://doi.org/10.1029/2006gc001488.
Ferguson, J., Henderson, G., Fa, D., Finlayson, J., Charnley, N., 2011. Increased seasonality in the Western Mediterranean during the last glacial from limpet shell geochemistry. Earth Planet. Sci. Lett. 308, 325–333.
Friedman, I., O'Neill, J., 1977. Compilation of Stable Isotope Fractionation Factors of Geochemical Interest. In: Data of Geochemistry, pp. 1–12.
Fry, B., 2002. Conservative mixing of stable isotopes across estuarine salinity gradients: a conceptual framework for monitoring watershed influences on downstream fisheries production. Estuaries 25, 264–271.
García-March, J.R., Surge, D., Lees, J.M., Kersting, D.K., 2011. Ecological information and water mass properties in the Mediterranean recorded by stable isotope ratios in *Pinna nobilis* shells. Journal of Geophysical Research: Biogeosciences 116.
Gillett, N., Kell, T., Jones, P., 2006. Regional climate impacts of the Southern Annular Mode. Geophys. Res. Lett. 33, 720.
Gillikin, D., Lorrain, A., Bouillon, S., Dehairs, F., Willenz, P., 2010. $\delta^{13}C$ in *Mytilus edulis* shells: relation to salinity, DIC, phytoplankton and metabolism. Org. Geochem. 37 (10), 1371–1382.
Gmelin, J., 1791. Caroli a Linnaei Systema Naturae per Regna Tria Naturae, Ed. 13. pp. 3021–3910 Tome 1(6), G.E. Beer, Lipsiae [Leipzig].
Gonfiantini, R., Stichler, W., Rozanski, K., 1995. Standards and intercomparison materials distributed by the International Atomic Energy Agency for stable isotope measurements. In: the Isotope Hydrology Section of the International Atomic Energy Agency (Ed.), References and Intercomparison Materials for Stable Isotopes of Light Elements. IAEA, Vienna, Austria, pp. 13–29.
Gong, D., Wang, S., 1999. Definition of Antarctic oscillation index. Geophys. Res. Lett. 26, 459–462.
Goodwin, D., Flessa, K., Schöne, B., Dettman, D., 2001. Cross-calibration of daily growth increments, stable isotope variation, and temperature in the Gulf of California bivalve mollusk *Chione cortezi*: Implications for paleoenvironmental analysis. Palaios 16, 387–398.
Goodwin, D., Schöne, B., Dettman, D., 2003. Resolution and fidelity of oxygen isotopes as paleotemperature proxies in bivalve mollusk shells: Models and observations. Palaios 18, 110–125.
Gordillo, S., Bujalesky, G., Pirazzoli, P., Rabassa, J., Saliège, J., 1992. Holocene raised beaches along the northern coast of the Beagle Channel, Tierra del Fuego, Argentina. Palaeogeogr. Palaeoclimatol. Palaeoecol. 99, 41–54.
Gordillo, S., Brey, T., Beyer, K., Lomovasky, B., 2015. Climatic and environmental changes during the middle to late Holocene in southern South America: a sclerochronological approach using the bivalve *Retrotarpes exalbidus* (*Dillwyn*) from the Beagle Channel. Quat. Int. 377, 83–90.
Graniero, L., Surge, D., Gillikin, D., Briz i Godino, I., Álvarez, M., 2016. Assessing elemental ratios as a paleotemperature proxy in the calcite shells of patelloid limpets. Palaeogeogr. Palaeoclimatol. Palaeoecol. 465, 386–395.
Grossman, E., Ku, T., 1986. Oxygen and carbon isotope fractionation in biogenic aragonite: Temperature effects. Chem. Geol. 59, 59–74.
Henry, R., Saintsing, D., 1983. Carbonic-anhydrase activity and ion regulation in 3 species of osmoregulating bivalve mollusks. Physiol. Zool. 56, 274–280.
Hickson, J., Johnson, A., Heaton, T., Balson, P., 1999. The shell of the Queen Scallop *Aequipecten opercularis* (L.) as a promising tool for palaeoenvironmental reconstruction: evidence and reasons for equilibrium stable-isotope incorporation. Palaeogeogr. Palaeoclimatol. Palaeoecol. 154, 325–337.
Jenkins, S., Hartnoll, R., 2001. Food supply, grazing activity and growth rate in the limpet *Patella vulgata* L.: a comparison between exposed and sheltered shores. J. Exp. Mar. Biol. Ecol. 258, 123–139.
Jones, D., 1983. Sclerochronology: reading the record of the molluscan shell. Am. Sci. 71, 384–391.
Jones, D., Quitmyer, I., 1996. Marking time with bivalve shells: oxygen isotopes and season of annual increment formation. Palaios 11, 340–346.
Jones, D., Williams, D., Arthur, M., Krantz, D., 1984. Interpreting the paleoenvironmental, paleoclimatic, and life history records in mollusc shells. Geobios Mem. Spec. 8, 333–339.
Jones, D., Williams, D., Romanek, C., 1986. Life history of symbiont-bearing giant clams from stable isotope profiles. Science 231, 46–48.
Jones, D., Arthur, M., Allard, D., 1989. Sclerochronological records of temperature and growth from shells of *Mercenaria mercenaria* from Narragansett Bay, Rhode Island. Mar. Biol. 102, 225–234.
Jones, D., Quitmyer, I., Arnold, W., Marelli, D., 1990. Annual shell banding, age, and growth rate of hardclams (*Mercenaria spp.*) from Florida. J. Shellfish Res. 9, 215–225.
Killingley, J., Newman, W., 1982. ^{18}O fractionation in barnacle calcite: a barnacle paleotemperature equation. J. Mar. Res. 40, 893–902.
Krantz, D., Williams, D., Jones, D., 1987. Ecological and paleoenvironmental information using stable isotope profiles from living and fossil molluscs. Palaeogeogr. Palaeoclimatol. Palaeoecol. 58, 249–266.
Land, L., Lang, J., Barnes, D., 1977. On the stable carbon and oxygen isotopic composition of some shallow water, ahermatypic, scleractinian coral skeletons. Geochim. Cosmochim. Acta 41, 169–172.
Lewis, J., Bowman, R., 1975. Local habitat-induced variations in the population dynamics of *Patella vulgata* L. J. Exp. Mar. Biol. Ecol. 17, 165–204.
Limpasuvan, V., Hartmann, D.L., 1999. Eddies and the annular modes of climate variability. Geophys. Res. Lett. 26 (20), 3133–3136 (792).
Lutz, R., Rhoads, D., 1977. Anaerobiosis and a theory of growth line formation. Science 198, 1222–1227.
MacClintock, C., 1967. Shell structure of Patelloid and Bellerophontoid gastropods (Mollusca). Peabody Mus. Nat. History Bull. 22 (140 pp).
Marshall, G., 2003. Trends in the Southern Annular Mode from observations and reanalyses. J. Clim. 16, 4134–4143.
Mauquoy, D., Blaauw, M., van Geel, B., Borromei, A., Quattrocchio, M., Chambers, F.M., Possnert, G., 2004. Late Holocene climatic changes in Tierra del Fuego based on multiproxy analyses of peat deposits. Quat. Res. 61, 148–158.
McConnaughey, T., 1989a. ^{13}C and ^{18}O isotopic disequilibrium in biological carbonates: patterns, I. Geochim. Cosmochim. Acta 53, 151–162.
McConnaughey, T., 1989b. ^{13}C and ^{18}O isotopic disequilibrium in biological carbonates: II. In vitro simulation of kinetic isotope effects. Geochim. Cosmochim. Acta 53, 163–171.
McCrea, J.M., 1950. On the isotopic chemistry of carbonates and a paleotemperature scale. J. Chem. Phys. 18, 849–857.
Morriconi, E., 1999. Reproductive Biology of the Limpet *Nacella* (*P.*) *Deaurata* (Gmelin, 1791) in Bahía Lapataia (Beagle Channel). Sci. Mar. 63 (S1), 417–426.
Morriconi, E., 2005. Tesis Doctoral: Ecología reproductiva de molusco gastrópodos del canal de Beagle. Universidad Nacional de La Plata.
Morriconi, E., Calvo, J., 1993. Environmental influence on shell allometric growth in *Nacella* (*Patinigera*) *deaurata* (Gmelin, 1791) from the Beagle Channel, Argentina. Malacologia 35.1, 135–140.
Moss, D.K., Ivany, L.C., Judd, E.J., Cummings, P.W., Bearden, C.E., Kim, W.-J., Artruc, E.G., Driscoll, J.R., 2016. Lifespan, growth rate, and body size across latitude in marine Bivalvia, with implications for Phanerozoic evolution. Proc. R. Soc. B Biol. Sci. 283, 20161364.
Orquera, L.A., Piana, E.L., 2009. Sea nomads of the Beagle Channel in southernmost South America: over six thousand years of coastal adaptation and stability. The Journal of Island and Coastal Archaeology 4, 61–81.
Orquera, L.A., Legoupil, D., Piana, E.L., 2011. Littoral adaptation at the southern end of South America. Quat. Int. 239, 61–69.
Pannella, G., MacClintock, C., 1968. Biological and environmental rhythms reflected in molluscan shell growth. In: Macurda, D.B., Paleontol, J. (Eds.), Paleobiological Aspects of Growth and Development, a Symposium, Paleontol. Soc. Mem., vol. 2. 42(5). pp. 64–80 suppl.
Parker, W., Yanes, Y., Surge, D., Mesa-Hernández, E., 2017. Calibration of the oxygen isotope ratios of the gastropods *Patella candei crenata* and *Phorcus atratus* as high-resolution paleothermometers from the subtropical eastern Atlantic Ocean. Palaeogeogr. Palaeoclimatol. Palaeoecol. 487, 251–259.
Ponce, J.F., Borromei, A.M., Menounos, B., Rabassa, J., 2017. Late-Holocene and Little Ice Age palaeoenvironmental change inferred from pollen analysis, Isla de los Estados, Argentina. Quat. Int. 442, 26–34.
Prendergast, A., Schöne, B., 2017. Oxygen isotopes from limpet shells: Implications for palaeothermometry and seasonal shellfish foraging studies in the Mediterranean. Palaeogeogr. Palaeoclimatol. Palaeoecol. 1–15.
Prothero, D., Schwab, F., 1996. Sedimentary Geology: An Introduction to Sedimentary Rocks and Stratigraphy, 1st ed. W. H. Freeman, New York 575 pp.
Rosenfeld, S., Marambio, J., Ojeda, J., Rodriguez, J., Gonzalez-Wevar, C., Gerard, G., Contador, T., Pizarro, G., Mansilla, A., 2018. Trophic ecology of two co-existing subantarctic limpets of the Genus *Nacella*: spatio-temporal variation in food availability and diet composition of *Nacella Magellanica* and *N. Deaurata*. ZooKeys 738, 1–25.
Schifano, G., Censi, P., 1983. Oxygen isotope composition and rate of growth of *Patella coerulea*, *Monodonta turbinata* and *M. articulata* shells from the western coast of Sicily. Palaeogeogr. Palaeoclimatol. Palaeoecol. 42, 305–311.
Schifano, G., Censi, P., 1986. Oxygen and carbon isotope composition, magnesium and strontium contents of calcite from a subtidal *Patella coerulea* shell. Chem. Geol. 58, 325–331.
Schöne, B., Dunca, E., Fiebig, J., Pfeiffer, M., 2005a. Mutvei's solution: an ideal agent for resolving microgrowth structures of biogenic carbonates. Palaeogeogr. Palaeoclimatol. Palaeoecol. 228, 149–166.
Schöne, B., Houk, S., Freyre Castro, A., Fiebig, J., Oschmann, W., Kroenke, I., Dreyer, W., Gosselck, F., 2005b. Daily growth rates in shells of *Arctica islandica*: Assessing subseasonal environmental controls on a long-lived bivalve mollusk. Palaios 20, 78–92.
Schöne, B., Rodland, D., Wehrmann, A., Heidel, B., Oschmann, W., Zhang, Z., Fiebig, J., Beck, L., 2007. Combined sclerochronologic and oxygen isotope analysis of gastropod shells (*Gibbula cineraria*, North Sea): Life history traits and utility as a high-resolution environmental archive for kelp forests. Mar. Biol. 150 (6), 1237–1252.
Sen Gupta, A., England, M., 2006. Coupled ocean–atmosphere–ice response to variations in the Southern Annular Mode. J. Clim. 19, 4457–4486.
Shackleton, N., 1973. Oxygen isotope analysis as a means of determining season of occupation of prehistoric midden sites. Archaeometry 15, 133–141.
Smith, H., Delafontaine, M., Flemming, B., 1988. Intertidal barnacles—Assessment of their use as paleo-environment indicators using Mg, Sr, $^{18}O/^{16}O$ and $^{13}C/^{12}C$ variations. Chem. Geol. 73, 211–220.
Smith, J., Schwarcz, H., Risk, M., McConnaughey, T., Keller, N., 2000. Paleotemperatures from deep-sea corals: overcoming "vital effects". Palaios 15, 25–32.
Spalding, M., Fox, H., Allen, G., Davidson, N., Ferdana, Z., Finlayson, M., Halpern, B., Jorge, M., Lombana, A., Lourie, S., Martin, K., McManus, E., Molnar, J., Recchia, C., Robertson, J., 2007. Marine ecoregions of the world: a bioregionalization of coastal and shelf areas. BioScience 57, 573–583.
Spero, H., Lea, D., 1996. Experimental determination of stable isotope variability in *Globigerina bulloides*: Implications for paleoceanographic reconstructions. Mar.Microorg. 28, 231–246.
Spero, H., Bijma, J., Lea, D., Bemis, B., 1997. Effect of seawater carbonate concentration on foraminiferal carbon and oxygen isotopes. Nature 390, 497–500.

Surge, D., Barrett, J., 2012. Marine climatic seasonality during medieval times (10th to 12th centuries) based on isotopic records in Viking Age shells from Orkney, Scotland. Palaeogeogr. Palaeoclimatol. Palaeoecol. 350-352, 236–246.
Surge, D., Walker, K., 2006. Geochemical variation in microstructural shell layers of the southern quahog (*Mercenaria campechiensis*): implications for reconstructing seasonality. Palaeogeogr. Palaeoclimatol. Palaeoecol. 237 (2–4), 182–190.
Surge, D., Lohmann, K.C., Dettman, D., 2001. Controls on the isotopic chemistry of the American oyster, *Crassostrea virginica*: Implications for growth patterns. Palaeogeogr. Palaeoclimatol. Palaeoecol. 172, 283–296.
Surge, D., Wang, T., Gutierrez-Zugasti, I., Kelley, P., 2013. Isotope sclerochronology of annual growth line formation in limpet shells (*Patella vulgata*) from warm and cold temperate zones in the eastern North Atlantic. Palaios 28, 386–393.
Swart, P., 1983. Carbon and oxygen isotope fractionation in scleractinian corals: a review. Earth Sci. Rev. 19, 51–80.
Tarutani, T., Clayton, R., Mayeda, T., 1969. The effect of polymorphism and magnesium substitution on oxygen isotope fractionation between calcium carbonate and water. Geochim. Cosmochim. Acta 33, 987–996.
Thompson, D., Solomon, S., 2002. Interpretation of recent Southern Hemisphere climate change. Science 296 (5569), 895–899.
Usdowski, E., Hoefs, J., 1993. Oxygen isotope exchange between carbonic acid, bicarbonate, carbonate, and water: a re-examination of the data of McCrea [1950] and an expression for the overall partitioning of oxygen isotopes between the carbonate species and water. Geochim. Cosmochim. Acta 57, 3815–3818.
Valdovinos, C., Ruth, M., 2005. Lapas Nacellidae del extreme sur de Sudamerica: taxonomıa y distribucion. Rev. Chil. Hist. Nat. 78, 497–517.
Vila, A., Mameli, L., Terradas, X., Estevez, J., Moreno, F., Verdún, E., Zurro, D., Clemente, I., Piqué, R., Briz, I., Barcelo, J.A., 2007. Ethnoarchaeological research in Tierra del Fuego (1986-2006): thoughts for European prehistoric archaeology. Trab. Prehist. 64, 37–53.
Wang, T., Surge, D., Mithen, S., 2012. Seasonal temperature variability of the Neoglacial (3300–2500 BP) and Roman Warm Period (2500–1600 BP) reconstructed from oxygen isotope ratios of limpet shells (Patella vulgata), Northwest Scotland. Palaeogeogr. Palaeoclimatol. Palaeoecol. 317-318, 104–113.
Wefer, G., Berger, W., 1980a. Stable isotopes in benthic foraminifera: Seasonal variation in large tropical species. Science 209, 803–805.
Wefer, G., Berger, W., 1980b. Growth histories of Strombid snails from Bermuda recorded in their O-18 and C-13 profiles. Mar. Biol. 60, 129–135.
Wefer, G., Berger, W., 1981. Stable isotope composition of benthic calcareous algae from Bermuda. J. Sediment. Petrol. 51, 459–465.
Wefer, G., Berger, W., 1991. Isotope paleontology: growth and composition of extant calcareous species. Mar. Geol. 100, 207–248.
Wefer, G., Killingley, J.S., 1980. Growth histories of strombid snails from Bermuda recorded in their O-18 and C-13 profiles. Mar. Biol. 60 (2), 129–135. https://doi.org/10.1007/BF00389156.
Weidman, C., Jones, G., Lohmann, K.C., 1994. The long-lived mollusk *Arctica islandica*: a new paleoceanographic tool for the reconstruction of bottom temperatures for the continental shelves of the northern North Atlantic Ocean. J. Geophys. Res. 99, 18,305–18,314.
Wheeler, A., 1992. Mechanisms of molluscan shell formation. In: Calcification in Biological Systems, pp. 179–216.
Zeebe, R., 1999. An explanation of the effect of seawater carbonate concentration on foraminiferal oxygen isotopes. Geochim. Cosmochim. Acta 63, 2001–2007.
Zurro, D., Negre, J., Pérez, J.R., Álvarez, M., Godino, I.B., Caro, J., 2017. An Ethnoarchaeological study on anthropic markers from a Shell-midden in Tierra del Fuego (Southern Argentina): Lanashuaia II. Environ. Archaeol. 22, 394–411.